Phase Transitions in Antimony Oxides and Related Glasses

Robin George Orman
B.Sc. (Hons.)

A thesis submitted to the University of Warwick in partial fulfilment of the requirement for the degree of Master of Science

Department of Physics September 2005

This work is dedicated to my friends Donna Carroll and Phillip Petcher

Contents

List of Figures

List of Tables

List of Abbreviations

DSC	Differential Scanning Calorimetry
DTA	Differential Thermal Analysis
EDX	Energy Dispersive X-ray Analysis
ICSD	Inorganic Crystal Structure Database
M-O-M	Metal-Oxygen-Metal
M-OH	Metal-Hydroxyl group
NMR	Nuclear Magnetic Resonance
SEM	Scanning Electron Microscope
STA	Simultaneous Thermal/Thermogravimetric Analysis
TGA	Thermogravimetric Analysis
XRD	X-ray Diffraction

Acknowledgements

I would like to thank the many people who have assisted me during the course of preparing this work, some of whom deserve special mention.

First and foremost amongst these is my supervisor, Dr Diane Holland, for her wisdom, patience and encouragement at all stages of my research. I must also thank various lab technicians with whom I have been privileged to work: Martin Davis for assistance with XRD, Steve York for help with SEM/EDX, and in particular to Dave Hammond and Keith Briggs for their invaluable technical expertise in too many areas to list.

I am also grateful to Dr Mark Newton and Mr Robin Cruddace for the use of (and instruction in using) the Raman spectrometer, and to Professor Frank Berry and Mr Xiaolin Ren at the Open University for their assistance in preparing valentinite by mechanical milling, and for the use of their equipment in doing so.

My thanks also to the other members of the Glass-Ceramics group, including Emma and James for sharing an office with me for the best part of a year (particularly during the writing of this thesis!). I owe many thanks to Ben Parkinson for the same reason, as well as for his guidance and tuition in the many nuances of glass research.

Finally, I wish to thank my parents for their understanding and support (financial and otherwise) throughout this first year of my postgraduate research career.

Declaration

The work for this thesis was carried out in the Department of Physics at the University of Warwick, unless otherwise stated. The work was completed during the period from September 2004 to September 2005 and, except where specifically acknowledged in the text, is the result of my own independent research and has not been previously submitted at the University of Warwick, or any other institution, in respect of a higher degree.

1st September 2005

Date

Robin Orman

Summary

This investigation aimed to clarify the phase transitions of antimony trioxide (Sb_2O_3) described in the literature, and to use the insights thus acquired to aid similar analyses on water- and chlorine-stabilised Sb_2O_3 glass samples. Simultaneous Differential Thermal/Thermogravimetric Analysis (STA), X-ray Diffraction (XRD) and Raman spectroscopy were some of the experimental approaches used. An understanding of the thermal behaviour of Sb_2O_3-based glasses would be beneficial in preparing them for commercial use; other heavy metal oxide glasses have exhibited non-linear optical properties and an extended infrared transmission region.

XRD and STA analysis revealed that the α-β phase transition in the crystalline Sb_2O_3 system tends to occur as a two-stage process, the first stage of which is apparently depressed by the presence of water. Other discrepancies with literature values are also thought to be related to contamination by water or other materials. Evidence that milling Sb_2O_3 depresses phase transitions – possibly by increasing the strain in the crystallites – was also found.

Water-stabilised antimony trioxide samples formed by pouring into water contained approximately 52% vitreous material. The crystalline material initially present and that formed on crystallisation of the glass exhibited similar behaviour to the crystalline oxides, with transitions apparently depressed by the presence of water.

Raman analysis of the chlorine-stabilised Sb_2O_3 glasses suggests an overall structure similar to that of onoratoite, and water-treatment revealed a sensitivity to moisture. Calculated activation energies for crystallisation using Kissinger plots and DSC measurements suggested a decrease in glass stability with age, possibly due to the introduction of hydroxyl groups. STA data showed depression of phase transitions as in the other two systems, probably due to the combined presence of chlorine and water in the samples.

Chapter 1

Introduction

1.1 Overview

Antimony oxides have been investigated in several studies by various authors in the last century. Their uses include acting as promoters for catalysts used for selective partial oxidations of hydrocarbons, and for related reactions such as oxidative coupling. However, the literature remains unclear on some aspects of their thermal phase transitions.

Predicted to be a glassformer in 1932 [1], attempts have been made to form a vitreous antimony trioxide glass, and are detailed in the literature [2-8]. However the 'pure' Sb_2O_3 glasses formed thus far all appear to be the result of the introduction of an unintended contaminant (principally SiO_2; *q.v.* Section 3.2.1), and hence some question remains as to the feasibility of actually producing a single-component antimony trioxide glass. Although not as yet investigated in depth, vitreous preparations of antimony trioxide have also been reported with the use of other stabilisers, including chlorine [9-11] and water [4].

The properties of these 'impure' Sb_2O_3 glasses may prove both interesting and useful; other heavy metal oxide glasses have exhibited an extended infrared transmission region as well as non-linear optical properties. However, the uncertainties that remain over the behaviour of crystalline Sb_2O_3 hamper further investigation into these glasses.

1.2 Aim of the work

The objective of this work has been two-fold. Firstly, it was necessary to conduct investigations into the thermal phase transitions of the two polymorphs of antimony trioxide in order to clarify and corroborate, or correct, the data already published in the literature. This information was then used to aid analyses of similar studies on the transitions of the water- and chlorine-stabilised glasses mentioned in Section 1.1. The ultimate aim was to characterise the thermal behaviour of both the crystalline antimony trioxide and the related vitreous systems.

A multi-technique approach was adopted for this work, and included thermal analysis measurements (DTA, STA and DSC) and structural studies (XRD, EDX, Raman spectroscopy).

1.3 Thesis structure

This thesis consists of six chapters of which this is the first, serving as an introduction to the main body of the work presented in the subsequent sections.

The second chapter outlines the background theory to glass systems and their behaviour, whilst Chapter 3 reviews the currently published work on crystalline antimony trioxide and the relevant vitreous systems. Chapter 4 briefly summarises the experimental techniques used in this investigation, and the conditions under which they were applied.

Chapter 5 details the experimental results obtained, together with analyses and discussion. This section will focus primarily on the thermal measurements detailing the phase transitions, aided by the characterisation of the materials from x-ray diffraction and Raman spectroscopy.

Finally, Chapter 6 summarises the conclusions that can be drawn from the experimental data and presents some suggestions for future investigations.

The reader should note that references quoted in the text are listed at the end of each chapter.

1.4 References

[1] W.H. Zachariasen, *J. Amer. Chem. Soc.* **54** (1932), 3841-3851.

[2] J.F. Bednarik and J.A. Neely, *Glastechn. Ber.* **55** (1982), 126-129.

[3] H. Masuda, Y. Ohta and K. Morinaga, *J. Japan Inst. Metals* **59**(1) (1995), 31-36.

[4] O. Borgen and J. Krogh-Moe, *Acta Chem. Scand.* **10**(2) (1956), 265-267.

[5] H. Hasegawa, M. Sone and M. Imaoka, *Phys. Chem. Glasses* **19**(2) (1978), 28-33.

[6] Y.P. Kutsenko, I.D. Turyanitsa and D.V. Chepur, *Fiz.-Khim. Stekla* **5**(4) (1978), 395-398.

[7] P.J. Miller and C.A. Cody, *Spectrochim. Acta* **38A**(5) (1982), 555-559.

[8] K. Terashima, T. Hashimoto, T. Uchino, S-H. Kim and T. Yoko, *J. Ceram. Soc. Japan* **104**(11) (1996), 1008-1014.

[9] A.C. Hannon, R.G. Orman and D. Holland, *J. Non-Cryst. Solids* (in preparation).

[10] J.A. Johnson, D. Holland, J. Urquidi, I.A. Gee, C.J. Benmore and C.E. Johnson, *J. Phys.: Condens. Matter* **15** (2003), 4679-4693.

[11] J.A. Johnson, D. Holland, J. Bland, C.E. Johnson and M.F. Thomas, *J. Phys.: Condens. Matter* **15** (2003), 755-764.

Chapter 2

Structure and Theory of Glasses

2.1 Glass definition and properties

We know from analysis of ancient Egyptian glassware that glasses have been manufactured by humans since at least 7000 BC. Sand – silica – was probably the first material used for glassmaking but, despite the fact that many modern glasses incorporate silica in their structure, it is not an essential component of a glass. In fact, a diverse array of chemical substances can be vitrified; materials are instead characterised as a glass based on their properties, rather than their composition.

A solid is generally characterised as a glass if it meets two criteria: it has no long-range order in its atomic arrangement, and it experiences a 'glass transformation region' (a time-dependent behaviour over a temperature range). This can best be explained with the aid of an enthalpy (or volume) vs. temperature plot (Fig. 2.01).

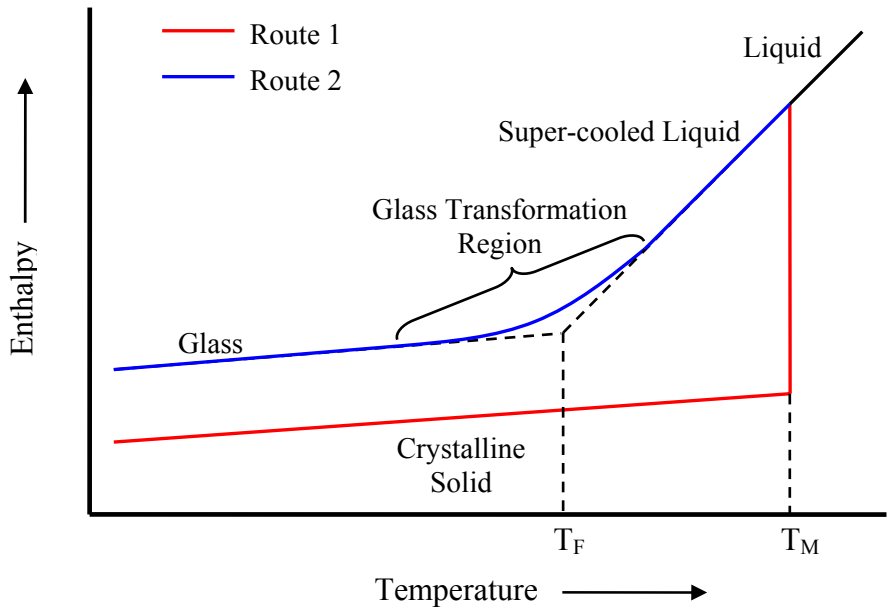

Figure 2.01 *– Thermodynamic diagram showing the changes in enthalpy of a glassforming liquid with temperature (route 2), as opposed to that of a normal liquid-solid transition (route 1). The fictive temperature, T_F, is the point at which the structure of the glass is considered to be that of the equilibrium liquid at that temperature [1].*

Consider a liquid at a temperature above its melting point. As the temperature is lowered, the enthalpy of the substance will gradually decrease and its atomic arrangement will slowly change, being at any point characteristic of the temperature of the melt. When the liquid is cooled below its melting point T_M it will generally experience an abrupt shift to a crystalline solid (with long-range atomic order) along with a correspondingly sharp decrease in enthalpy (route 1).

However, if the liquid can be cooled below the melting point without crystallisation ('super-cooled') it will continue to exhibit a gradual decrease in enthalpy with temperature (route 2). As cooling progresses, the viscosity of the liquid will increase; at some point the viscosity will be such that the atomic structure of the liquid will be unable to realign to the equilibrium arrangement for its temperature in the time available. This will cause the enthalpy of the system to increasingly lag from the equilibrium line until the point is reached where the viscosity prevents *any* further atomic rearrangement. In essence, the liquid has become an (amorphous) solid with no long-range order – one of the conditions for a material to be considered as a glass. In addition, the process of super-cooling has also fulfilled the second requirement: the temperature region lying between the enthalpy being that of the equilibrium liquid and that of the frozen liquid is what is known as the *glass transformation region*.

As indicated, the glass transformation region exists over a range of temperatures. However, it is often useful to define a single, *glass transition temperature*, T_g, as an indication of the onset of the glass transformation region on heating the glass. This is defined empirically, and the value obtained for a given glass is dependent on several factors, including the rate at which the melt was originally cooled to form the glass, the experimental method used to determine T_g and the heating rate applied. Hence, T_g should not be a considered a true property of the glass, but is a useful indicator of when the transition between glass and supercooled liquid occurs.

Finally, it should be noted that, whilst cooling of a melt is perhaps the most common method of glassmaking, it is by no means the only way of doing so: chemical vapour deposition and sol-gel processing are examples of other such techniques.

2.2 Glass-forming Oxides and Chlorides

Silica, SiO_2, is one of a series of oxides known as 'glass-formers' (or 'network formers') that will readily form glasses on their own – other examples are B_2O_3, GeO_2 and P_2O_5. The cations in these oxides tend to form highly covalent bonds with oxygen, which has been shown to be a common feature of glassformers. Oxides with cations whose oxygen bonding is more ionic in nature – such as SeO_2, WO_3 and Al_2O_3 – will not form a glass on their own, but will do so when melted with a suitable quantity of a second oxide; these are termed 'intermediates' or 'conditional glassformers'. Finally, oxides formed from highly ionic bonds never form a glass, but can be used to affect the glass structure created from other glassformers. These oxides are known as 'modifiers'.

Oxyhalide and metal halide systems can also be glassformers. Of the latter, zinc chloride is one of the most widely studied, since it has a tetrahedral structure similar to that of silica.

2.3 Simple structural theories of glass formation

Different chemical systems require specific cooling rates to be met or exceeded in order to form glasses. This fact has led to several attempts to produce a complete atomic theory of glass formation based on the nature of the chemical bonds and the shape of the structural units involved. Whilst it may seem strange to propose structural theories for a substance that is defined as having 'no long-range, periodic atomic ordering', it has been found to be possible to reproducibly form the same glass from a nominal starting composition, implying that there is some form of 'short-range' ordering present that is sufficient to control the overall properties.

In 1926, Goldschmidt presented a theory of glass formation for the general A_2O_3 system based on the empirical observation that these most readily formed glasses when the cation-oxygen radius ratio was between 0.2 and 0.4. Since values in this range tend to produce cations surrounded by oxygen atoms in a tetrahedral arrangement, Goldschmidt posited that this atomic structuring was most favourable for glass formation. However, this theory has been subsequently shown to be incomplete, with a variety of systems inadequately explained by it.

Six years later Zachariasen [2] extended Goldschmidt's ideas and produced perhaps the most cited paper in glass science. Zachariasen noted that silicate crystals, which readily form glasses, have network structures instead of the close-packed

tetrahedral arrangement described by Goldschmidt. By postulating that the oxygen polyhedra found in the oxide crystals would also be present in the glasses, Zachariasen formed the concept of a continuous random network structure for a glass, with periodic structural arrangement prevented by random orientations. These can be achieved by variations in bond angles and bond lengths, or by rotation of structural units (Fig. 2.02).

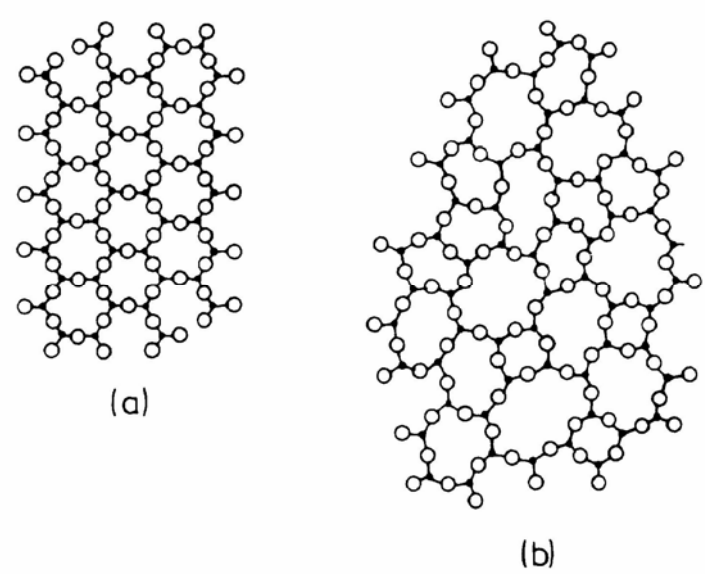

Figure 2.02 *– A schematic 2D representation of (a) a generic A_2O_3 crystalline compound and (b) a continuous random network of the same substance [3].*

Zachariasen also proposed a set of rules to allow for this structure:

1) No oxygen atom must be linked to more than two cations.
2) The number of oxygen atoms surrounding any given cation must be small (typically 3 or 4).
3) Oxygen polyhedra share only corners, not edges or faces.

A fourth rule was added to ensure that the network would be three-dimensional (although certain glasses can exist in structures describable in fewer dimensions):

4) At least three corners of each oxygen polyhedron must be shared.

Some exceptions to these rules do exist, but they have still formed the basis for most widely-used models of glass structure since.

2.4 Phase separation in glasses

When oil is poured into water, the two liquids will spontaneously separate into two layers, the less dense fluid floating on the surface of the other. This happens because oil and water are *immiscible*, and the resulting mixture is *phase-separated*.

The same process can occur in a glass melt. If the oil/water mixture already mentioned were to be shaken vigorously in a sealed container, droplets of the minority fluid would be visible suspended in the other. These droplets would then rise or fall as appropriate to form the phase-separated layers. However, the rate of this separation would be dependent on the viscosity of the two fluids, which is inversely proportional to the temperature. In a glass melt which is rapidly cooled, it is not uncommon for droplets of one immiscible component to nucleate in a matrix of another, producing a phase-separated glass (the two components might also form separate layers, if sufficiently fluid). The droplets in such a glass are not always visible to the unaided eye, and other techniques such as electron microscopy are necessary to observe the effect.

Phase-separation can have significant effects on the thermal and chemical stability of the glass and can also be used, in the 'separated layers' case, to produce two types of glass, each with distinct properties, from the same melt.

2.5 Multi-component glasses: structure and stability

Whilst some glassformers form vitreous systems on their own with relative ease (e.g. B_2O_3, P_2O_5, etc.), other, poorer glassformers require more extreme cooling rates for this to occur (e.g. As_2O_3 and, it seems probable, Sb_2O_3; *q.v.* Section 3.2.1). As detailed in Section 2.3 above, glass structural theories require the formation of a continuous random network of atoms, as opposed to the ordered, repeating atomic arrangement in a crystal lattice – this can be made to occur more readily in poor glassformers by adding a small amount of a contaminant.

In terms of enthalpy, glasses are thermodynamically less favourable than the available crystalline modifications (*q.v.* Fig. 2.01); however, their random structures are more entropic. The trade-off between reducing the enthalpy and decreasing the entropy during crystallisation is prevented by kinetic factors: once a supercooled liquid drops below T_g the activation energy necessary to reform the structure (Fig. 2.03) is no longer present, and the atoms become locked in an amorphous arrangement. The ease with

which a melt forms a crystal lattice is also affected by kinetics, since crystals form by a process of nucleation and growth.

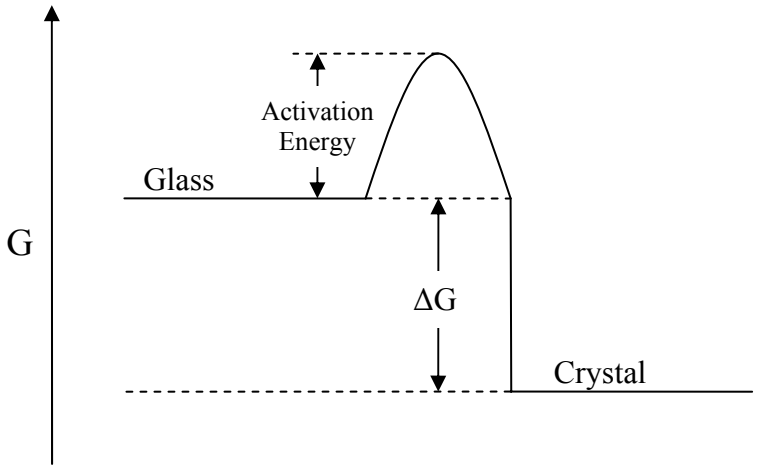

Figure 2.03 *– Free energy diagram showing how a glass, although thermodynamically less stable, can be prevented from crystallising by the absence of the required activation energy.*

The introduction of a contaminant increases the overall entropy of the system – making it somewhat less thermodynamically favourable to form a crystal structure – and hinders the kinetic realignment by providing more bonds to break and atoms to rearrange, frustrating crystal formation. Thus, the presence of a contaminant in a melt can substantially improve the glassforming ability of a system.

However, such impurities can also play a significant role in the properties of the glass formed – a particularly important factor when considering that not all contamination is intentional: melting in certain crucibles may introduce additional impurities to a mixture, for example. Another common contaminant is water which forms hydroxyl groups in the glass structure, and is difficult to regulate between preparations.

Glass melts are cooled by a variety of techniques, depending on the glass to be formed and its stability; less stable glasses require more extreme cooling techniques. Splat-quenching (pressing the melt between two cooled metal plates), roller-quenching (pouring the melt between two rotating cylinders) and melt-spinning (forcing a thin stream of melt onto a roller to quench, with the aid of high-pressure gas) are some examples of methods used, and offer cooling rates on the order of 10^3, 10^6 and 10^8 °C/min, respectively.

2.6 Summary

A glass can be considered as the result of lowering the temperature of a supercooled liquid to the point at which it becomes too viscous to reach an equilibrium arrangement in a realistic time period; in other words, at that point the energy of the system is insufficient to allow a thermodynamically favourable drop in enthalpy to occur kinetically. The resulting amorphous structure can be modelled as a continuous random network, with no long-range periodic ordering, although short-range atomic alignments characteristic of the material still appear to exist and regulate the properties of the glass.

Substances can be classified as glassformers, intermediates or modifiers by their ability (or lack thereof) to form a glass, either alone or in concert with another component. The degree of ease with which a glassformer can be used to form a vitreous system can be improved with the addition of a contaminant, although this can also affect the properties of the resulting glass.

2.7 References

[1] J.E. Shelby, *Introduction to Glass Science and Technology*, Royal Society of Chemistry, 1997.

[2] W.H. Zachariasen, *J. Amer. Chem. Soc.* **54** (1932), 3841-3851.

[3] A. Paul, *Chemistry of Glasses*, Chapman & Hall, 1990.

Chapter 3

Literature Review of Antimony Oxides and Related Glasses

3.1 Antimony Oxides

3.1.1 Introduction

Antimony oxides exist in several forms including antimony trioxide (Sb_2O_3), antimony tetroxide (Sb_2O_4) and antimony pentoxide (Sb_2O_5). Of these, Sb_2O_3 occurs as either a cubic or an orthorhombic polymorph (commonly known as senarmontite and valentinite respectively), whilst Sb_2O_4 can be monoclinic (clinocervantite) or, more commonly, orthorhombic (cervantite). Antimony tetroxide is a mixed valency compound, containing both Sb^{3+} and Sb^{5+} ions in equal proportions in its crystal lattice [1] and is stable to around 1000°C [2], the exact value depending upon atmosphere and the method of sample preparation [3].

It is worth noting that the 'molecular' structure of senarmontite (Fig. 3.01a) does not appear to lend itself to glass formation when compared with the 'double-chain' structure of valentinite (Fig. 3.01b) which can be expected to form the 'continuous random network' outlined by Zachariasen [4] with greater ease. Also, the similarities between the structures of valentinite and cervantite (Fig. 3.01c) have been shown to be relevant to the oxidation process, discussed later (*q.v.* Section 3.1.3).

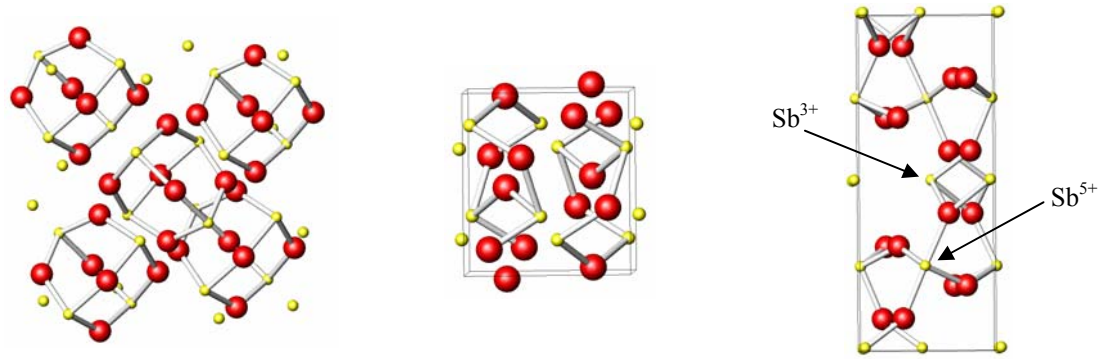

Figure 3.01 *– The structures of (a) senarmontite, (b) valentinite and, (c) cervantite. Sb^{3+} forms $[Sb_2O_3]$ trigonal pyramids to accommodate the lone pair of electrons whilst Sb^{5+} (in cervantite) occupies $[SbO_6]$ octahedra.*

Thermal studies of antimony oxides have been undertaken by several researchers, but there is a lack of consistency in the data obtained, particularly as regards the two polymorphs of Sb_2O_3. Reports on antimony trioxide and relevant related glasses are considered in the following sections – it should be noted that this discussion will be revisited in Chapter 6 in light of the data obtained from this work.

3.1.2 The Senarmontite-Valentinite Transition

Whilst orthorhombic valentinite is generally regarded as the high-temperature stable polymorph of antimony trioxide, the solid-solid transition temperature from cubic senarmontite (the low-temperature stable form) is a matter of some dispute in the literature (Table 3.01).

Temperature (°C)	Year	Reference
570 ± 10	1928	5
606 ± 5	1967	6
600 ± 10	1975	7
629	1981 & 1989	1,2
640-655	1987	8
556	1988	9
606	1993	10

Table 3.01 – The senarmontite-valentinite transition temperature, as determined by various authors.

In 1928, Roberts and Fenwick [5] determined its value to be (570 ± 10)°C, although the Sb_2O_3 used in their experiment was initially found to contain a high sulphide content and the subsequent purification process may have affected their results. This is also supported by a lack of consistency with later estimates.

Jones *et al.* [8] calculated a value of 650°C from thermodynamic data, and empirically confirmed both that the transition had occurred at or before this point, and that it appeared to be inseparable from the subsequent melting of the valentinite thus formed (in the range 640-655°C). It was also determined that heating valentinite above 600°C provided the activation energy necessary to transform to the more thermodynamically stable senarmontite.

Centers [9] in 1988 quoted a temperature of 556°C for the transition, although this appears to have been an unsupported assertion and later notes in the same work indicate that orthorhombic Sb_2O_3 was prepared through heat treatment in the range 625-640°C, rather than at the lower value.

As an aside, it should be noted that Berry and Ren [11] reported that the transition from senarmontite to valentinite (and from α-Sb_2O_4 to β-Sb_2O_4) could also be induced, without direct heating, through mechanical processes in a planetary ball mill. It can be surmised that localised heating sufficient for the transition to take place occurs during mechanical collisions within the high-energy system, and this process has potential benefits for producing finely-ground valentinite from pure or mixed senarmontite samples, avoiding the problems of volatilisation [1-3] and oxidation (*q.v.* Section 3.1.3)

3.1.3 Polymorph Oxidation Temperatures

Senarmontite Oxidation Temperature (°C)	Valentinite Oxidation Temperature (°C)	Mixture Oxidation Temperature (°C)	Reference
575	463	–	2
500-660	450-540	–	3
510*		–	7
460	400	380	12

Table 3.02 – The oxidation temperatures of senarmontite, valentinite and mixtures of the two polymorphs, as determined by various authors.
* The polymorph(s) present in this sample of Sb_2O_3 was not specified by the authors.

The low oxidation temperature of valentinite with respect to senarmontite has been noted by several authors [2-3,12], and was explained by Trofimov *et al.* in their study of crystal orientation over the oxidation event [12] as being due to coherent linking of the Sb_2O_4 (cervantite) phase to the original valentinite matrix, substantially reducing the energy of nucleation. This topotactic growth process was later described in much greater detail by Gopalakrishnan and Manohar [13], supporting the earlier findings and the work of Centers [14] provided further support for the hypothesis that the oxidation of Sb_2O_3 is actually sublimation-controlled, with senarmontite subliming to low-energy valentinite nucleation sites before oxidising.

The impact of particulate size on oxidation has only been sparingly examined in the literature, and has largely been confined to the alleged impact on the oxidation temperatures of the different polymorphs [9]. It should be noted that there is little published evidence for this at present; in fact the opposite conclusion (that particulate size minimally affects oxidation) was drawn in another work [3]. In this latter case however, Cody *et al.* provided only nominal support for their position – in particular, particle size measurements were not included – and their argument appears to be based

purely on the use of multiple valentinite samples from the same supplier (NL Industries). However, the lower temperatures obtained by Trofimov *et al.* for the individual polymorphs may be attributable to the fine-grained nature of the trioxide used in the study.

Analysis of the oxidation process in antimony trioxide is further complicated by the simultaneous volatilisation that occurs. Several authors [2-3] have reported that this competing process tends to result in an overall gain in mass for valentinite (although this varies with heating rate) and a mass loss for senarmontite.

3.1.4 Melting Point of Sb_2O_3

The melting point of Sb_2O_3 is perhaps the least disputed thermal event of those mentioned, with a general consensus that it occurs soon after the senarmontite-valentinite phase transition, and a value of (655 ± 2)°C [9,12] is usually quoted in the literature. However, Golunski *et al.* [2] reported a temperature of (643 ± 2)°C in their study, whilst other authors [8] have reported that melting occurred between 640°C and 655°C, depending on heating rate.

3.2 Antimony Oxide-based Glasses

3.2.1 Single-component Antimony Oxide Glass

Antimony oxide was predicted to be a glassformer by Zachariasen in 1928 [4]. In the intervening period, several binary and ternary Sb_2O_3-based glasses have been studied, including various oxide [15-18] and halide [19-22] systems, and numerous attempts have been made to form single-component antimony oxide glasses [16-17,23-27]. These latter efforts have failed to provide conclusive evidence for such a glass however, with several methods of glass preparation prone to the introduction of contaminants during melting – principally silica [25-26] as determined by several authors [19-20,23,27]. In other studies, Masuda *et al.* [16] failed to obtain any pure Sb_2O_3 glass, whilst others deliberately introduced a small quantity of B_2O_3 [17] to stabilise the material.

The 'single-component' Sb_2O_3 glasses prepared to date have generally been determined to possess a structure most similar to that of valentinite, the high temperature crystalline polymorph [17,23,27], with studies such as that of Hasegawa *et al.* [17] that used x-ray diffraction analysis to obtain an Sb-O interatomic distance of

1.99Å, Sb-O co-ordination of 3.15 and an Sb-Sb distance of 2.8Å to support their conclusions. Occasional studies have also suggested structures based on senarmontite [24] and even vitreous As_2O_3 [26]. Studies of the thermal behaviour of these glasses have generally not been carried out, although Bednarik and Neely [28] obtained T_g and T_c values of 245°C and 296°C for their glass using a DSC technique.

3.2.2 Water-stabilised Antimony Oxide Glass

Another attempt to form a single component antimony oxide glass was undertaken by Borgen and Krogh-Moe in 1956 as part of a study of the modifications of As_2O_3 and Sb_2O_3 [24]. Although no explicit method is given for the glass preparation, the authors do mention that the glass was formed by "pouring [the] melted oxide into water"; Cody *et al.* later attempted, unsuccessfully, to duplicate this procedure [3].

Whilst the glass formed by Borgen and Krogh-Moe was treated as a single-component antimony oxide sample in the study, without a more detailed explanation of the method of preparation – and given the difficulties already established in forming such a glass – it seems more likely that some contamination (either the water or some impurity therein) was present that aided glass formation – this may also go some way to explaining the difficulty experienced in duplicating the preparation. Some support for this view comes from a recent experiment by Hannon and Holland [29] who, whilst attempting to form pure Sb_2O_3 glass, observed the formation of a small quantity of vitreous material from a melt which they deemed likely to be due to water entering the crucible during quenching.

Borgen and Krogh-Moe also concluded from their infrared spectra of the glass and the crystalline polymorphs that the glass structure was closest to that of senarmontite, rather than the valentinite-type structure generally agreed upon for the other 'pure' antimony oxide glasses discussed in Section 3.2.1.

3.2.3 Chlorine-stabilised Antimony Oxide Glass

Whilst investigating Sb_2O_3-$ZnCl_2$ glasses [21-22], Johnson *et al.* attempted to form a single component antimony oxide glass from 50 mol% Sb_2O_3 and 50 mol% $SbCl_3$ – the resultant glass was initially determined to have no detectable chlorine content. However, further work by Hannon *et al.* [20] established that approximately 8 at% of the contaminant remained within the glass structure. The properties and thermal

behaviour of this chlorine-stabilised antimony oxide glass have not as yet been studied in any depth.

3.3 Summary

The thermal events upon heating crystalline antimony trioxide, whilst the subject of several studies, remain a matter of some dispute, in particular with regard to the senarmontite-valentinite (α-Sb_2O_3 to β-Sb_2O_3) phase transition. Attempts to prepare a purely vitreous form of the trioxide have so far met with failure, although glasses containing small amounts of a contaminant (SiO_2 from heating the melt in silica containers being the most common) have been created. Recent work has produced a chlorine-stabilised variant of the trioxide glass, the properties of which have yet to be investigated. A 'pure' Sb_2O_3 glass obtained by pouring the melt into cold water has also been reported in the literature, but it seems likely that such a preparation will incorporate water, or a related impurity, in a similar fashion to the above glasses. The structures of the glasses mentioned are either unknown or disputed, although the majority suggest an arrangement most similar to that of crystalline valentinite.

3.4 References

[1] S.E. Golunski and D. Jackson, *Appl. Catal.* **48** (1989), 123-135.

[2] S.E. Golunski, T.G. Nevell and M.I. Pope, *Thermochim. Acta* **51** (1981), 153-168.

[3] C.A. Cody, L. DiCarlo and R.K. Darlington, *Inorg. Chem.* **18**(6) (1979), 1572-1576.

[4] W.H. Zachariasen, *J. Amer. Chem. Soc.* **54** (1932), 3841-3851.

[5] E.J. Roberts and F. Fenwick, *J. Amer. Chem. Soc.* **50** (1928), 2125-2147.

[6] W.B. White, F. Dachille and R. Roy, *Z. Krist.* **125** (1967), 450-458.

[7] Y.K. Agrawal, A.L. Shashimohan and A.B. Biswas, *J. Therm. Anal.* **7** (1975), 635-641.

[8] S.A. Jones, J. Fenerty and J. Pearce, *Thermochim. Acta* **114** (1987), 61-66.

[9] P.W. Centers, *J. Solid State Chem.* **72** (1988), 303-308.

[10] I. Barin, *Thermochemical Data of Pure Substances, Second Edition*, VCH, 1993.

[11] F.J. Berry and X. Ren, *J. Mater. Sci.* **39** (2004), 1179-1183.

[12] V.G. Trofimov, A.I. Sheinkman and G.V. Kleshchev, *Izv. Vyssh. Uchebn. Zaved. Fiz.* **3** (1973), 135-137.

[13] P. Gopalakrishnan and H. Manohar, *Pramana* **3** (1974), 277-285.

[14] P.W. Centers, R.L. Wright, F.D. Price and C.J. Klenke, *Phys. Chem. Glasses* **30**(4) (1989), 149-150.

[15] M. Nalin, M. Poulain, M. Poulain, S.J.L. Ribeiro and Y. Messaddeq, *J. Non-Cryst. Solids* **284** (2001), 110-116.

[16] H. Masuda, Y. Ohta and K. Morinaga, *J. Japan Inst. Metals* **59**(1) (1995), 31-36.

[17] H. Hasegawa, M. Sone and M. Imaoka, *Phys. Chem. Glasses* **19**(2) (1978), 28-33.

[18] P. Charton, P. Thomas and P. Armand, *J. Non-Cryst. Solids* **321** (2003), 81-88.

[19] B. Dubois, H. Aomi, J.J. Videau, J. Portier and P. Haggenmuller, *Mater. Res. Bull.* **19** (1984), 1317-1323.

[20] A.C. Hannon, R.G. Orman and D. Holland, *J. Non-Cryst. Solids* (in preparation).

[21] J.A. Johnson, D. Holland, J. Urquidi, I.A. Gee, C.J. Benmore and C.E. Johnson, *J. Phys.: Condens. Matter* **15** (2003), 4679-4693.

[22] J.A. Johnson, D. Holland, J. Bland, C.E. Johnson and M.F. Thomas, *J. Phys.: Condens. Matter* **15** (2003), 755-764.

[23] J.F. Bednarik and J.A. Neely, *Glastechn. Ber.* **55** (1982), 126-129.

[24] O. Borgen and J. Krogh-Moe, *Acta Chem. Scand.* **10**(2) (1956), 265-267.

[25] Y.P. Kutsenko, I.D. Turyanitsa and D.V. Chepur, *Fiz.-Khim. Stekla* **5**(4) (1978), 395-398.

[26] P.J. Miller and C.A. Cody, *Spectrochim. Acta* **38A**(5) (1982), 555-559.

[27] K. Terashima, T. Hashimoto, T. Uchino, S-H. Kim and T. Yoko, *J. Ceram. Soc. Japan* **104**(11) (1996), 1008-1014.

[28] J.F. Bednarik and J.A. Neely, *Phys. Chem. Glasses* **23**(6) (1982), 204-205.

[29] A.C. Hannon and D. Holland (personal communication).

Chapter 4

Experimental Theory and Practice

4.1 Sample Preparation

4.1.1 Introduction

In addition to the glassmaking of the water- and chlorine-stabilised glasses, it was necessary to synthesise pure samples of onoratoite ($Sb_8O_{11}Cl_2$; for comparison with the chlorine-stabilised glasses) and each of the polymorphs of Sb_2O_3, where these were not available commercially. It should be noted that all samples were stored under vacuum in a desiccator between measurements, as a precaution to avoid any further reaction than necessary with oxygen or atmospheric moisture.

4.1.2 Crystalline Antimony Trioxide

Commercial antimony trioxide (99.6%, Alfa Aesar) was obtained, and was used as the basis for preparation of a pure valentinite sample by mechanical milling, following the method laid out by Berry and Ren [1]: 18g of commercial Sb_2O_3 was dry milled in a Retsch PM 400 planetary ball mill using stainless steel balls and vials (250ml capacity) at 200rpm, with a 1:20 powder to ball weight ratio[1]. Milling was undertaken for 6 hours, the time period chosen to coincide with the first XRD spectrum found by Berry and Ren to be pure valentinite. An XRD scan later confirmed that the powder produced by this method was pure valentinite (*q.v.* Section 5.1.1).

An earlier attempt to duplicate the above method with a vibrational mill in place of a planetary ball mill also took place, and the resulting powder was retained for characterisation; XRD analysis later identified this powder as unchanged from the commercial Sb_2O_3 (*q.v.* Section 5.1.1). However, this sample was retained for investigation due to the reduced particulate size expected from its preparation (compared with the commercial sample).

For the purposes of clarity, it should be noted that the latter sample will henceforth bear the prefix “milled” when discussed, whilst the valentinite sample will

[1] The preparation of this sample was carried out at the Open University, Milton Keynes, in collaboration with Dr Frank Berry and Xiaolin Ren.

be preceded by the term “mechanically-derived”. The purchased antimony trioxide will be referred to as the “commercial” sample.

4.1.3 Onoratoite ($Sb_8O_{11}Cl_2$)

Since a commercial supplier of onoratoite could not be found, a sample was prepared from antimony trichloride (99%, Sigma-Aldrich) based on a preparation outlined by Matsuzaki *et al.* [2]. 20g of $SbCl_3$ was hydrolysed in 200ml of water at 35°C, precipitating $Sb_4O_5Cl_2$. The precipitate was then washed with ethyl ether in a fume cupboard and left to stand overnight on a hot plate at 70°C both to dry the powder and to allow any remaining ether to evaporate safely. Following confirmation of sample purity by x-ray diffraction, the $Sb_4O_5Cl_2$ was heated in a tube furnace under flowing argon to 420°C, held for one hour, then allowed to cool below 100°C before retrieval. X-ray diffraction confirmed the resulting powder to be pure onoratoite (*q.v.* Section 5.1.1) within the limits of detection.

4.1.4 Water-quenched Antimony Oxide Glasses

Based on previous work by Borgen and Krogh-Moe [3], attempts were made to form an Sb_2O_3 glass by pouring the molten oxide into water to quench. Two 25g batches of Sb_2O_3 powder (99.6%, Alfa Aesar) in lidded alumina crucibles were placed directly into a furnace at 800°C and 1050°C respectively, and held at temperature for 6 minutes. The 800°C mix was barely molten after this time, and was returned to an 850°C furnace for a further 5 minutes; the 1050°C melt required no additional time. Both preparations were quenched by pouring into room temperature deionised water contained in a stainless steel bucket.

4.1.5 Chlorine-stabilised Antimony Oxide Glasses

Three chlorine-stabilised antimony oxide glasses were prepared from Sb_2O_3 (99.6%, Alfa Aesar) and $SbCl_3$ (99%, Sigma-Aldrich) according to the nominal stoichiometry $xSb_2O_3(1\text{-}x)SbCl_3$ with x = 0.5, 0.7 and 0.85 (Table 4.01). The powders were mixed, placed in a lidded alumina crucible (to reduce the loss of volatile components) and placed into a furnace that had been heated to 1000˚C. The mixture was held at temperature for 5-10 minutes until molten and fuming, before being agitated and splat-quenched between two cooled copper plates. This process was based on a

previous study of the Sb_2O_3-$PbCl_3$-$ZnCl_2$ glass system [4]; chemical analysis had shown that there was no detectable contamination from alumina.

x (mole fraction)	weight% Sb_2O_3	weight% $SbCl_3$	50g	30g	15g
0.50	56.1	43.9	✓		
0.70	74.9	25.1		✓	✓
0.85	87.9	12.1		✓	✓

Table 4.01 – The percentage weight of each compound used to achieve the initial molar composition, and the batch masses used. Due to chlorine losses on heating, it was deemed impractical to attempt mixing based on the desired final glass composition.

The x = 0.5 glass prepared (by a similar method) and previously studied by Hannon *et al.* [5] was also examined in this work.

4.2 X-ray Analysis Techniques

4.2.1 X-ray Diffraction (XRD)

4.2.1.1 Introduction

X-rays incident on a substance will be scattered by the electrons in each atom of the material. Most of this scattering will interfere with itself destructively; if the substance has a crystal lattice structure however, diffraction will occur when rays scattered from the atomic planes at a given angle are in phase with each other. These scattered rays will constructively interfere to produce a strong signal in a detector placed at the appropriate position.

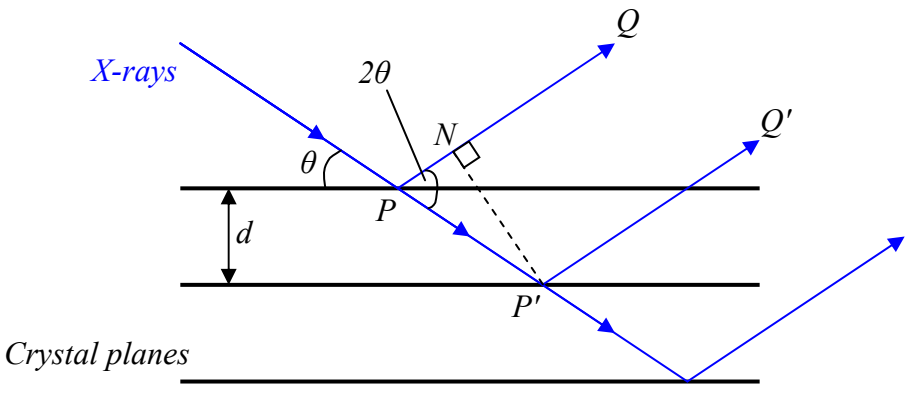

Figure 4.01 *– Schematic diagram of an x-ray beam incident on the planes of a crystal lattice.*

A beam of monochromatic x-rays is incident on the parallel planes of a crystal at an angle of θ (Fig. 4.01). For the diffracted beams PQ and $P'Q'$ to be in phase the path difference between them ($PP' - PN$) should be an integral multiple of the wavelength λ. Therefore

$$n\lambda = PP'(1-\cos 2\theta) = \frac{d}{\sin\theta}(1-\cos 2\theta)$$

which simplifies to give Bragg's Law,

$$n\lambda = 2d\sin\theta$$

Hence, any crystalline material will give strong bursts of diffracted x-rays as an x-ray source is swept along an angular path around it, as the angle of incidence fulfils the Bragg condition. Furthermore, plotting the intensity of the diffracted x-rays versus 2θ gives a series of peaks characteristic of the crystalline material, as determined by its atomic arrangement.

4.2.1.2 XRD of crystalline and glassy materials

With a crystal, the regular periodic arrangement of atomic planes gives sharp, discrete peaks at specific angles of incidence (Fig. 4.02) and the pattern of peaks obtained can be used to identify the substance.

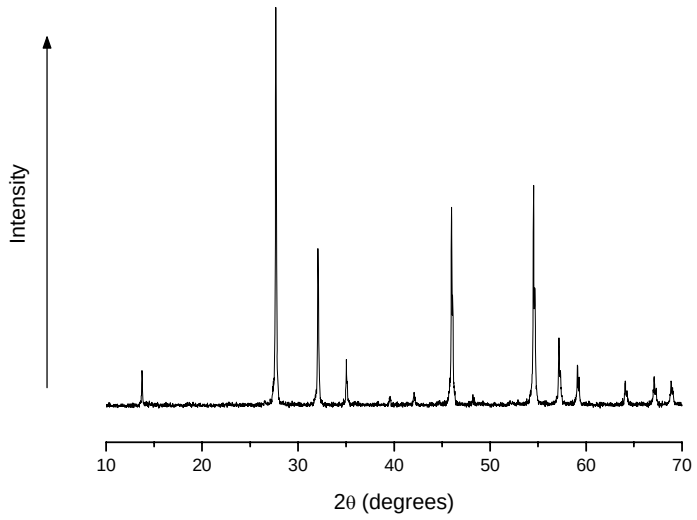

Figure 4.02 *– An example of the XRD pattern of a crystalline material.*

The amorphous nature of glassy materials makes such simple 'finger-printing' methods difficult: there is no long-range ordering of atomic planes to produce distinct peaks – instead, vitreous materials give broad diffraction peaks over large angular ranges (Fig. 4.03). However, XRD patterns of glasses remain useful to confirm the absence (or otherwise) of crystalline content in the sample.

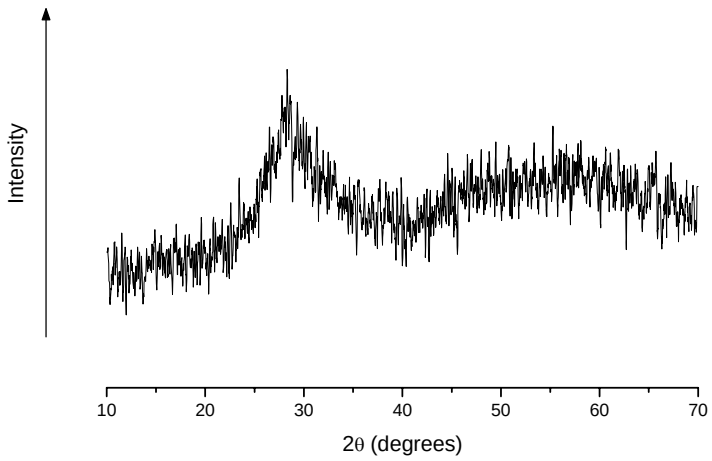

Figure 4.03 *– An example of the XRD trace of a glass (smoothed for clarity).*

X-ray diffraction patterns were obtained using a Bruker D5005 diffractometer with a constant 12mm footprint on the sample. Unless otherwise stated, all runs were over a 2θ range of 10-70° at 0.02° increments using a Cu K_α radiation source at 40kV-30mA (40kV-40mA for vitreous samples). Aluminium holders with a 20mm diameter circular sample area were used for most measurements (exceptions are noted) and any resulting aluminium diffraction peaks present in results are labelled. An acquisition time of 5 seconds per angular increment was used for all samples unless otherwise noted.

Note that all XRD spectra displayed in this work have been smoothed with a 5-point FFT algorithm. Where the experimental XRD patterns have been compared with the peaks established for specific substances, a reference to the relevant single crystal study has been given. The data therein were used to calculate the peak positions and intensities using the Inorganic Crystal Structure Database (ICSD) [6], and it is these lines that have been plotted.

4.2.2 Energy Dispersive X-ray Analysis (EDX)

Energy Dispersive X-ray analysis uses a high-energy (typically 10keV) electron beam to produce x-rays from a substance. The x-rays are produced by electrons decaying to fill vacancies in lower shells caused by the bombardment of the beam, and their energies are therefore characteristic of the elements present in the target material. Obtaining a spectrum of the relative counts of the detected x-rays versus their energies then allows quantitative measurements of the elements present and their relative abundance in the sample to be made.

A JEOL 6100 Scanning Electron Microscope and a 10kV accelerating voltage was used for all EDX measurements. ZAF corrections to the recorded x-ray emission spectra (correcting for the effects of atomic number, absorption and fluorescence of each atomic species on the emitted x-rays) were calculated with reference to a characterised internal standard: the behaviour of the species in the samples studied may not relate to these standards with total accuracy.

The effects of the limited penetration depth of the electron beam were minimised by analysis of powdered samples for quantitative measurements (sample fragments were also examined to obtain SEM images). However, with the possible inaccuracies in the ZAF corrections mentioned above, values obtained from this technique should be considered estimates only.

4.3 Thermal Analysis Techniques

4.3.1 Introduction and experimental methods

Transitions in a substance are often accompanied by changes in enthalpy and sometimes mass. Various thermal analysis techniques have been developed to investigate these events – which can include melting, oxidation, glass transitions, phase transitions, etc. – and the temperatures at which they occur. Knowledge of the thermal stability of materials is useful in a wide variety of studies including those into the hazards of storing explosives, the conditions for drying tobacco and other crops, the degradation of polymers, the shelf-life of drugs and, of course, the properties of amorphous materials.

Thermal Analysis is the measurement of changes in the physical properties of a substance as a function of temperature whilst the substance is subjected to a controlled temperature programme.

When studying a new material, thermal analysis techniques are best used in combination with each other to produce unambiguous results. For example, Thermogravimetric Analysis (TGA) of a sample cannot be used to detect melting, whilst melting and decomposition cannot be distinguished unambiguously using Differential Thermal Analysis (DTA). The use of complementary techniques such as all forms of spectroscopy, x-ray diffraction, electron microscopy, etc. are also of importance in characterising a new material, and their utilisation can also aid in identifying the thermal events occurring in a sample.

Unusual features on thermal analysis results can indicate equipment malfunction or unintentional contamination of the sample whilst preparing for measurement. Therefore, in this work, any thermal scans containing anomalies were repeated to confirm their existence (or otherwise).

4.3.2 Differential Thermal Analysis (DTA)

Differential Thermal Analysis (DTA) measures the difference in temperature between a sample and a reference material when both are subjected to the same heating program. If a thermal event (endothermic or exothermic) occurs in the sample its temperature, T_S, will either lag behind or precede (respectively) that of the reference, T_R. A graph of ΔT (= $T_S - T_R$) versus T_R shows thermal events as peaks with characteristic onset temperatures; the position of the peak tip is dependent on factors such as the heating rate and sample size – the area under each peak is related to the enthalpy change for the thermal event.

All DTA measurements in this work were carried out on a Stanton-Redcroft DTA 673-4 using a heating and cooling rate of 10°C/min, over the temperature range 30-800°C (unless otherwise stated). Samples were ground to a powder before loading into 90%Pt-10%Rh crucibles (approximate sample masses of 150mg were used), and quartz was used as a reference material. Atmospheres of flowing air and argon (at 250ml/min) have been used – the gas used for each dataset is specified. When running under argon, the inert gas was allowed to flow for 30 minutes before the start of the thermal program, to insure that all air had been purged from the system.

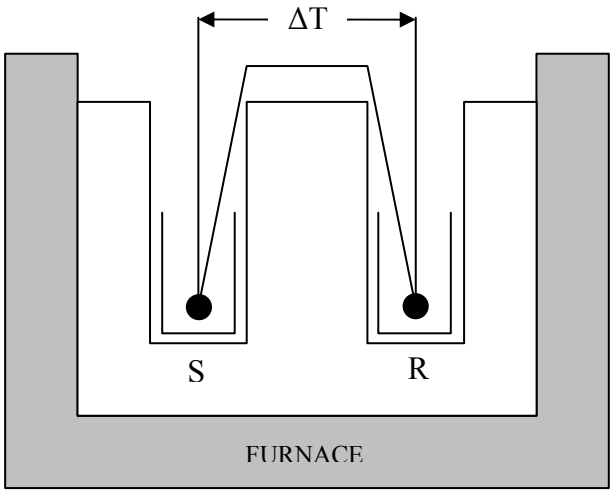

Figure 4.04 *– Schematic diagram of the DTA apparatus, showing the sample (S), reference (R) and differential temperature measurement. The block inside the furnace in which the crucibles reside is chosen to act as a suitable heat sink [7].*

Quartz was chosen as a reference material because it undergoes a single thermal event (onset at 574°C [8]) on heating and cooling, when it transforms between its α and β phases. The advantage of having this single-point check of the temperature scale was deemed to outweigh the potential problem posed by the (relatively small) transition peak obscuring other thermal events occurring in the sample.

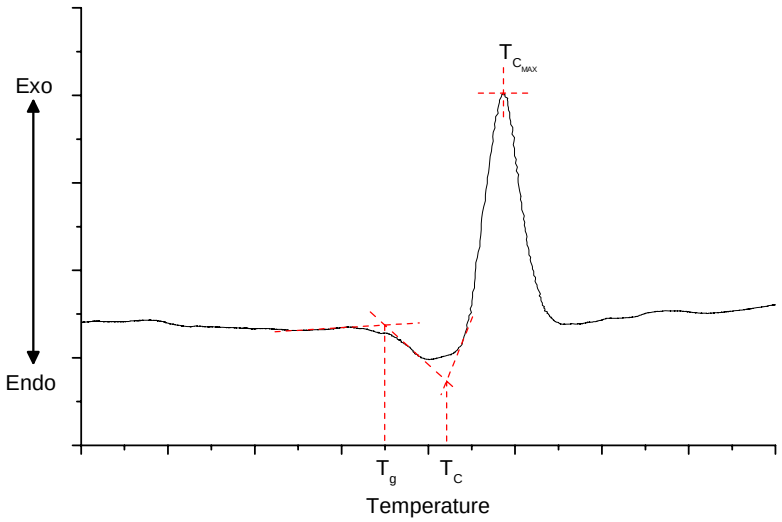

Figure 4.05 *– An example of a DTA curve with extrapolated glass transition and crystallisation temperatures. Note that extrapolated onset temperatures are quoted throughout this work, unless otherwise stated (as e.g.* $T_{C_{MAX}}$ *) since peak temperatures are often dependent on factors such as the heating rate used and the sample size.*

4.3.3 Differential Scanning Calorimetry (DSC)

Differential Scanning Calorimetry (DSC) is superficially similar to DTA, but differs in that it records the heat energy necessary to maintain the desired heating rate rather than the temperature difference. Unlike DTA, the sample and reference are placed in separate furnaces, and the temperature program is maintained by varying the power input to the two heating elements. The energy required to do this serves as a measure of the enthalpy changes in the sample relative to the reference (usually just an empty pan for DSC).

In this work, DSC measurements were carried out on a PerkinElmer Diamond DSC over the temperature range 30-500°C, using nitrogen as a purge gas at 20ml/min. Heating rates varied from 5 to 500°C/min, and aluminium or copper pans were used (the reference was an empty pan of the type used to hold the sample).

DSC data at different heating rates ϕ was used to prepare Kissinger plots of the crystallisation peak temperatures $T_{\max}$ to obtain the activation energy E. This involved plotting $\ln(\phi/T_{\max}^2)$ against $1/T_{\max}$ to give a line with gradient $-E/R$ (for a more detailed description of the Kissinger method, see [7]). More kinetic analysis of the samples was planned from the DSC measurements, but constraints imposed by the volatilisation of the samples under inert atmospheres above 500°C made this unfeasible in the time available.

4.3.4 Simultaneous Differential Thermal/Thermogravimetric Analysis (STA)

Whilst DTA and DSC techniques relate enthalpy changes in a sample with variations in temperature, Thermogravimetric Analysis (TGA) examines changes in mass. Whilst limited to examining thermal events where this occurs (typically desorption, decomposition and oxidation) in these situations TGA can often produce useful information, particularly regarding stable and meta-stable intermediates formed during a thermal process.

Simultaneous Thermal/Thermogravimetric Analysis (STA) combines the DTA and TGA techniques to give concurrent measurements. This makes drawing conclusions about the thermal behaviour of the sample significantly easier, whilst

avoiding the potential difficulties of preparing identical samples for analysis in parallel experiments.

A PerkinElmer Diamond TG/DTA system was used for all STA measurements, using either argon or air flowing at 200ml/min as a purge gas – as with the DTA, care was taken to purge the system of air before running under argon. Sample masses were typically 20-40mg and, as with DTA, a similar amount of quartz powder was used as a reference material. Heating rates varied from 10-160°C/min; the exact atmospheric and thermal conditions for each dataset are quoted where appropriate. Ten data points were collected per second at all heating rates.

For most samples in this work, DTA provided no further information to the STA measurements carried out (exceptions are of course noted) and often produced data of lower quality. Therefore STA measurements are used in most instances, and when such data is mentioned at low rates (10-20°C/min) it can be taken that DTA as outlined in Section 4.3.2 will produce very similar results.

Although datasets were collected under both flowing air and flowing argon, it often proved to be the case that oxidation in the former case (Fig. 4.06a) would obscure or conceal other features of interest, observable under argon (Fig. 4.06b). For this reason, many of the STA results discussed in Chapter 5 will be from those runs conducted under argon, and this should be assumed unless otherwise stated.

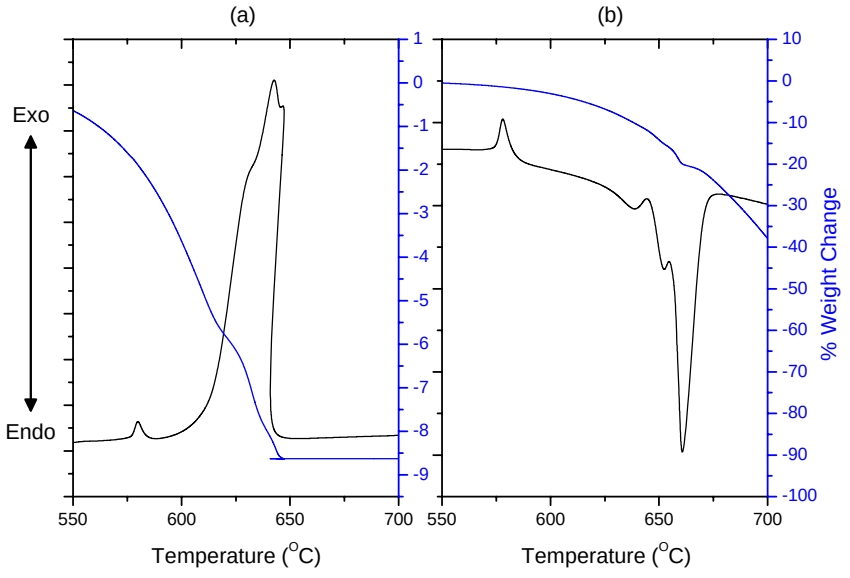

Figure 4.06 *– Comparison of the STA data obtained for a sample (a) under air and (b) under argon.*

Occasionally, when a thermal event is sufficiently exothermic, the sample temperature can lead the program temperature for short periods. This causes a 'sloping' effect on the heat flow and weight change curves (Fig. 4.07a) which can make them difficult to interpret; however, whilst plotting against program temperature gives a clearer graph (Fig. 4.07b), measurement of onset temperatures is then hampered by the sample being at a different temperature to that plotted. In this work, all plots are made against sample temperature, except where plotting versus program temperature shows the thermal behaviour more clearly; all measurements are taken from plots of sample temperature regardless, for accuracy.

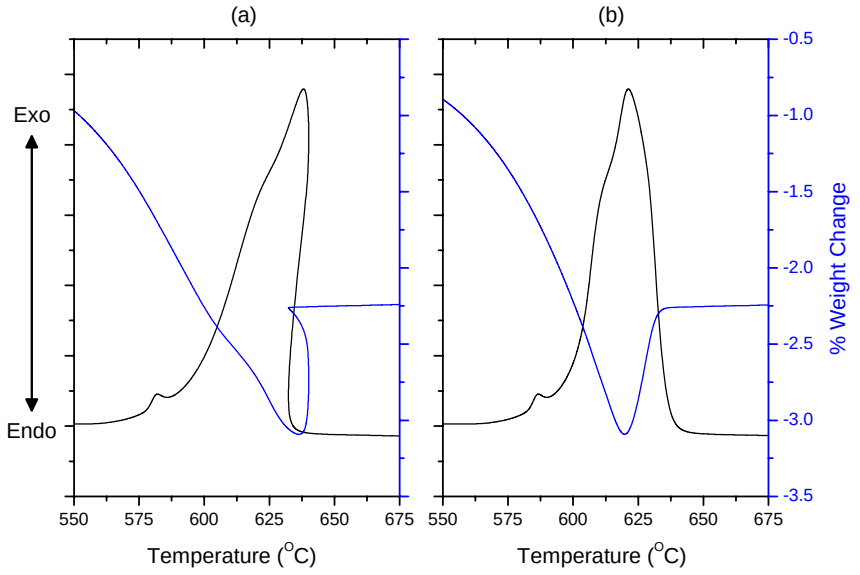

Figure 4.07 *– A comparison of the heat flow and weight change plotted against (a) sample temperature and (b) program temperature, for the same sample.*

4.4 Raman Spectroscopy [9-10]

When electromagnetic radiation is incident on a surface, some of it will be scattered. The majority of this scattered radiation will be of the same frequency as the incident beam ("Rayleigh scattering") – however, a certain minority of the scattered energy will be at discrete frequencies above and below that of the incident radiation ("Raman scattering").

Scattering can be explained in terms of the quantum theory of radiation. The incident radiation of frequency ν will consist of photons of discrete energies $h\nu$ (h is Planck's constant) and, as these photons impact on the molecules of the target surface,

scattering will occur. If the scattering is perfectly elastic the energy of the scattered photons will be unchanged, as will their frequency – this is Rayleigh scattering.

Should the photon-molecule collision be inelastic however, the energy change ΔE will be the difference between two of the allowed states of the molecule: in other words, ΔE must represent a change in the rotational or vibrational energy of the molecule. If the molecule is to gain energy, the photon must itself have an energy of $h\nu - \Delta E$ on scattering, and conversely, a $h\nu + \Delta E$ photon will scatter if the molecule loses energy during the collision. The frequency of the scattered radiation will also be $\nu - \Delta E/h$ or $\nu + \Delta E/h$, respectively.

Radiation scattered at a lower frequency in this manner is known as Stokes' radiation, whilst higher frequency scattering is called anti-Stokes' radiation. Since a decrease in molecular energy (anti-Stokes') can only occur if the molecule is already in an excited state, Stokes' scattering is the more common form – however, both forms of Raman scattering are still rare compared to Rayleigh scattering.

Since the Raman scattering process is not very efficient (approximately 1 in 10^7 of the incident photons will do so) a laser is required to act as the high power light source. The laser is also a monochromatic light source, so that all of the photons will initially have the same energy and will interact with the target molecules in the same way.

Raman spectra were obtained from a Renishaw Invia Raman spectrometer equipped with a 20mW laser source of wavelength 514nm. Measurements in this work were acquired with 10mW incident laser power with x50 magnification at room temperature. The number of acquisitions and the range of frequency shifts examined varied by sample – a 100-3200 cm^{-1} acquisition was first performed for each sample to establish appropriate settings – typical values were 5-10 acquisitions and a frequency shift range of 100-2000 cm^{-1}. The percentage power of the laser used was also varied to prevent peaks being truncated by saturation of the detector: 5% power was the lowest setting required, and was used for most samples.

Due to the localised nature of the Raman analysis (the spot analysed is approximately 10x10μm), minor variations in sample composition and geometry can cause changes in the spectra obtained for a single sample. To minimise this, three measurements were taken at different points on each sample, and the averaged spectrum was used for analysis.

4.5 References

[1] F.J. Berry and X. Ren, *J. Mater. Sci.* **39** (2004), 1179-1183.

[2] R. Matsuzaki and A. Sofue, Y. Saeki, *Chem. Lett.* **12** (1973), 1311-1314.

[3] O. Borgen and J. Krogh-Moe, *Acta Chem. Scand.* **10**(2) (1956), 265-267.

[4] M.R. Sahar, M.M. Ahmed and D. Holland, *Inst. Phys. Conf. Ser.* **111** (1990), 449-458.

[5] A.C. Hannon, R.G. Orman and D. Holland, *J. Non-Cryst. Solids* (in preparation).

[6] Inorganic Crystal Structure Database, Chemical Database Service, Daresbury Laboratory: http://cds.dl.ac.uk/cds/cds.shtml

[7] M.E. Brown, *Introduction to Thermal Analysis (Techniques and Applications)*, Chapman and Hall, 1988.

[8] I. Barin, *Thermochemical Data of Pure Substances, Second Edition*, VCH, 1993.

[9] C.N. Banwell, *Fundamentals of Molecular Spectroscopy, Third Edition*, McGraw-Hill, 1983.

[10] K. Nakamoto, *Infrared and Raman Spectra of Inorganic and Coordination Compounds (Part A: Theory and Applications in Inorganic Chemistry), 5th Edition*, Wiley-Interscience, 1997.

Chapter 5

Results and Discussion

5.1 Antimony Oxides

5.1.1 X-ray Diffraction

The four crystalline samples – antimony tetroxide (99.997%, Sigma-Aldrich), antimony trioxide (99.6%, Alfa Aesar) and the two mechanically-milled preparations thereof (*q.v.* Section 4.1.2) – were subjected to x-ray diffraction analysis to determine their phase purity.

X-ray diffraction characterised the commercial Sb_2O_4 as cervantite (Fig. 5.01a) – albeit with a small number of peaks that do not appear in the reference pattern. These peaks do not match either polymorph of Sb_2O_3, Sb_2O_4 or that of dry Sb_2O_5. The XRD scan of the commercial Sb_2O_3 characterised it as pure senarmontite, with no apparent valentinite (or other) peaks (Fig. 5.01b). To confirm the latter, a further sample consisting of 95% commercial Sb_2O_3 and 5% valentinite (by weight) was also examined (Fig. 5.02): from this it was readily apparent that the additional valentinite peaks were not detectable in the commercial material.

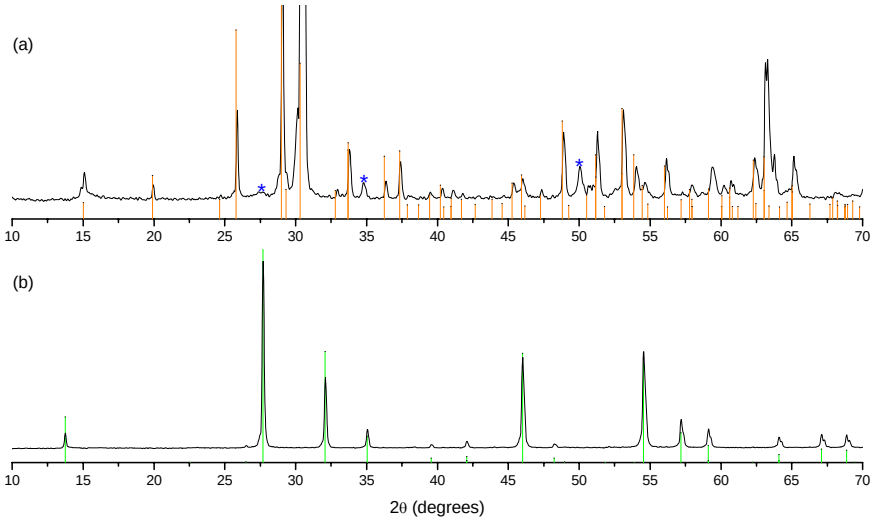

Figure 5.01 *– XRD patterns of (a) the commercial Sb_2O_4 and (b) the commercial Sb_2O_3. Reference peaks are also shown for cervantite (orange) [1] and senarmontite (green) [2], and some intense Sb_2O_4 peaks have been truncated. The starred peaks in (a) are discussed further in the main text.*

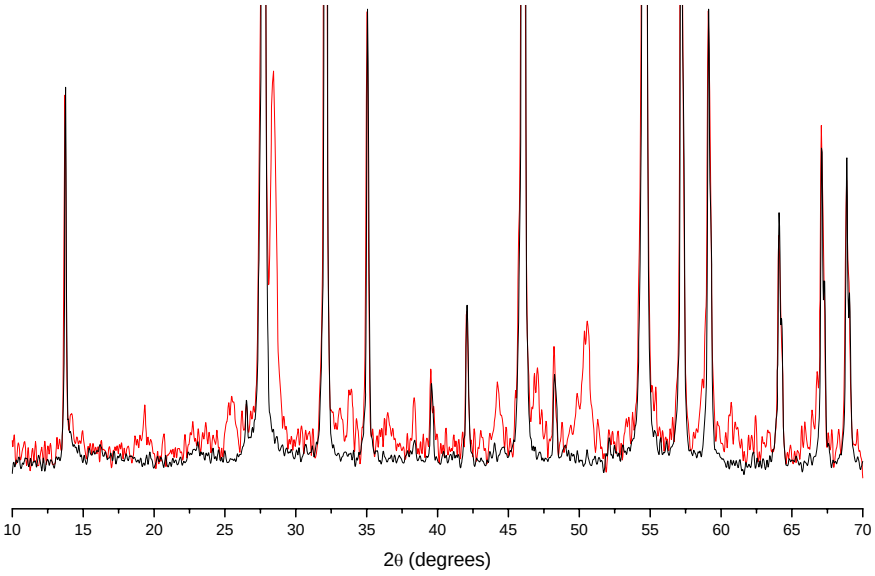

Figure 5.02 *– XRD pattern comparison of commercial Sb_2O_3 (black) and the same sample with 5 wt.% valentinite added (red). Some of the more intense senarmontite peaks have been truncated.*

The x-ray diffraction patterns of the mechanically milled samples showed that the antimony trioxide prepared in the vibrational mill remained pure senarmontite (Fig. 5.03a), whilst the Sb_2O_3 from the planetary ball mill had undergone the transition to valentinite (Fig. 5.03b). Neither sample displayed any peaks originating from the alternate polymorph. The onoratoite preparation (*q.v.* Section 4.1.3) produced pure onoratoite, with no peaks from the precursor ($Sb_4O_5Cl_2$) or the decomposition product (senarmontite) apparent (Fig. 5.03c).

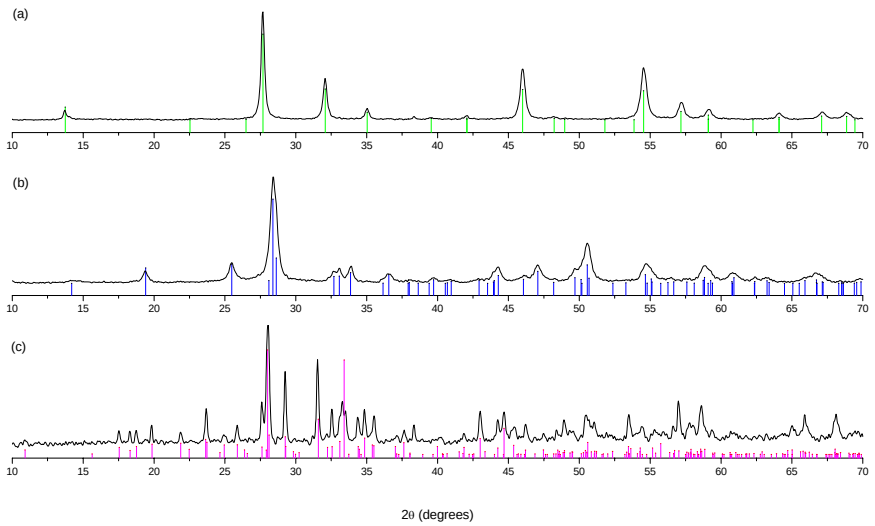

Figure 5.03 *– XRD patterns of the Sb_2O_3 samples (a) crushed in a vibrational mill and (b) pulverised in a planetary ball mill, and (c) the onoratoite preparation. Reference peaks for senarmontite (green) [2], valentinite (blue) [3] and onoratoite (magenta) [4] are also shown.*

The peaks obtained for the mechanically-derived valentinite were noticeably broader than for the other crystalline samples. These may be due to strain or crystallite size, so particle size measurements were carried out on the three Sb_2O_3 samples using a laser-scattering technique on a Malvern Mastersizer/E and propan-2-ol as a suspension liquid. An ultrasonic stirrer was also used in an attempt to break up agglomerates. The results are shown in Table 5.01; however the data is generally unhelpful since the powders showed a tendency to agglomerate.

Sample	Mean Particle Size (μm)	Range of sizes for 75% of particles (μm)
Commercial Sb_2O_3	4	1.5-10
Milled Senarmontite	3	0.6-7.0
Mechanically-derived Valentinite	3	0.5-8.0

Table 5.01 – Particle sizes measured for the three Sb_2O_3 crystalline samples.

5.1.2 Raman Spectroscopy

The Raman spectra for the mechanically-derived samples reinforce the species identification from the XRD results (Fig. 5.04), as do those of the commercial Sb_2O_3 (not shown, since it is identical to that of the milled senarmontite) and Sb_2O_4 samples (Fig. 5.05). The source of the extra peaks noted for the latter in the XRD spectrum do not appear to have affected the Raman analysis, and the peaks identified correlate well with those of other authors (as do those of the other samples; Table 5.02). Assignments of peaks to specific vibrations are not available in the literature.

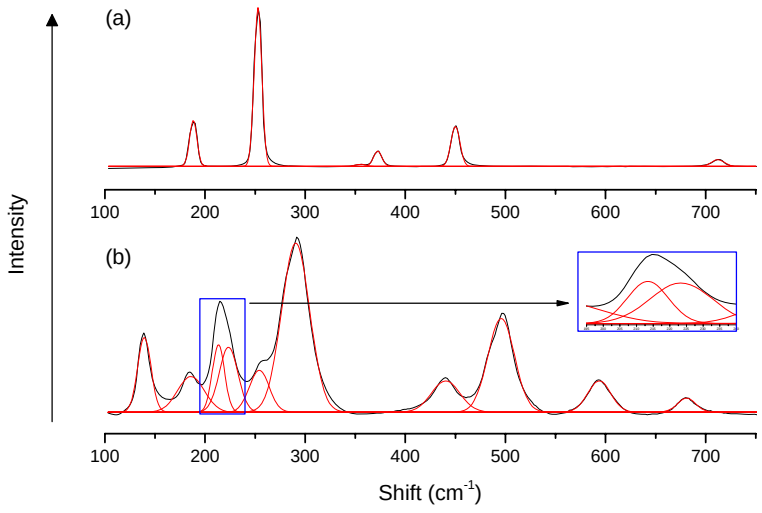

Figure 5.04 *– Raman spectra with peaks deconvoluted for commercial Sb_2O_3 (senarmontite) crushed in (a) a vibrational mill, and (b) a planetary ball mill. The peaks for the two samples match literature values for senarmontite and valentinite, respectively, within experimental error (Table 5.02). The inset shows why two overlapping peaks were fitted to one feature in the valentinite.*

Polymorph	This Work		Mestl *et al.* [5]		Cody *et al.* [6]		Terashima *et al.* [7]	
	Peak (cm^{-1} ±4)	Rel. Intensity	Peak (cm^{-1})	Rel. Intensity	Peak (cm^{-1})	Rel. Intensity	Peak (cm^{-1})	Rel. Intensity
Senarmontite			118		124	8.5	122	w
	188	29	189		197	53	193	s
	253	100	254	vs	261	100	258	vs
	355	1	355	sh	364	<1		
	372	10	373		381	7	377	s
	450	25	450		458	13.5	454	vs
							592	w
			684	sh				
	712	4	712		722	2	737	s
			904	vw				
Valentinite					103	5	109	w
	139	44	141		140	100	149	s
	186	21	189		194	15	193	w
	213	40	219					
	223	38			223	32.5	225	s
	254	25			269	sh		
	291	100	295		294	46	301	vs
	440	18			449	7	449	s
	496	55	500		502	24	505	vs
	594	19	596		602	8	600	s
	681	8			690	3	692	s
Cervantite					101	<1		
			117	vw				
					137	sh		
	142	6	142		140	30.5		
					192	sh		
	199	100	199		200	100		
					209	sh		
	218	9	221	sh	224	4		
	243	5	239	w	241	1.5		
			255	sh	255	6.5		
	261	17	262		263	16		
					274	<1		
	279	3	283		285	2		
	357	2	353					
					373	<1		
	399	26	400		403	30		
	408	11	413	sh	420	sh		
					455	sh		
	462	20	463		467	12.5		
	612	2	614					
	652	2	652					
	711	1	714		713	<1		
					730	<1		
	752	1	758		758	<1		
	823	2	825		819	<1		
					858	<1		

Table 5.02 – Comparison of the Raman peaks obtained from this work and in three others [5-7] over the shift range 100-1000cm^{-1}. The relative intensities of the peaks are listed as either percentages of the maximum amplitude, or as abbreviations (vs: very strong, s: strong, w: weak, vw: very weak, sh: shoulder).

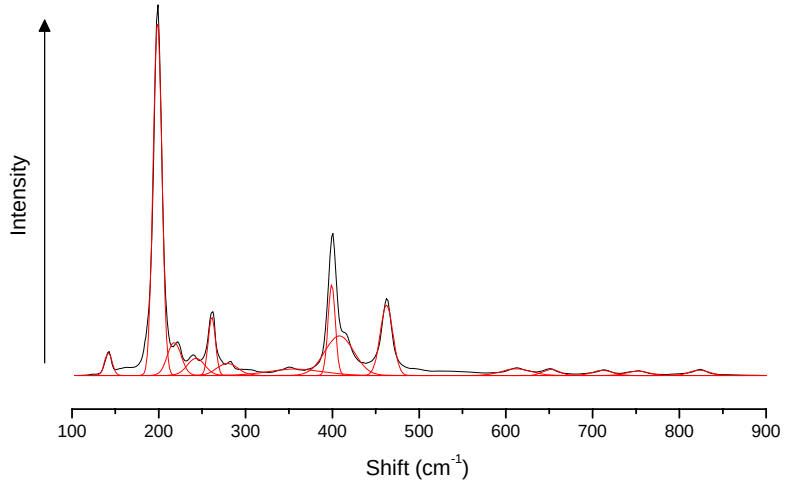

Figure 5.05 *– The Raman spectrum with peaks deconvoluted for the commercial Sb_2O_4 sample. Peak positions and relative intensities are listed in Table 5.02.*

5.1.3 Thermal Analysis

As expected, the cervantite sample was inert over the temperature range (up to 900°C) used for the measurements. STA traces of the two senarmontite samples under flowing argon are very similar, as could be expected (Fig. 5.06); however, each sample demonstrates a distinct thermal feature apparently not present in the other.

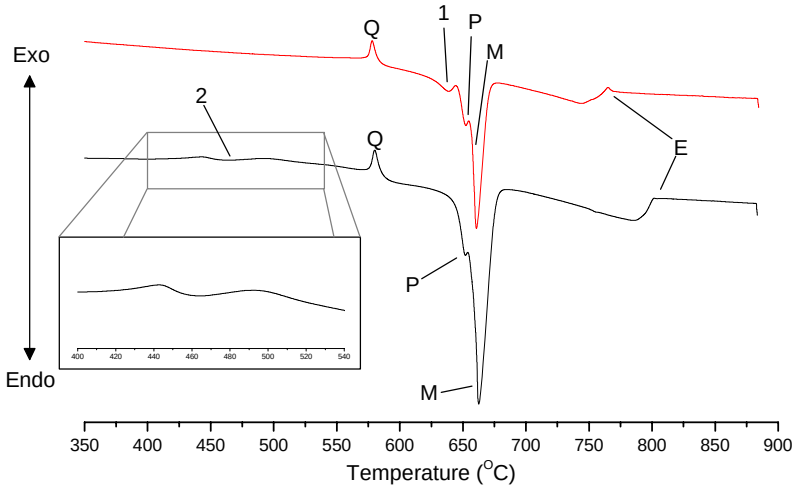

Figure 5.06 *– Comparison of the STA heat flow traces for the commercial and mechanically-milled senarmontite samples (red and black, respectively) at a heating rate of 20°C/min under flowing argon. Peak labels are as follows: Q = α-β quartz transition; P = senarmontite-valentinite phase transition; M = melting; E = end of volatilisation. Numbered peaks are discussed in more detail in the main text.*

In the commercial senarmontite, an additional endothermic peak, onset at 615±3°C (labelled as "Peak 1" in Figure 5.06) occurs before melting. Since only a single pre-melting peak was expected (that of the senarmontite-valentinite phase transition) a heat-treatment to 638°C was carried out to identify the nature of Peak 1; to make a reasonably accurate attempt at this without triggering a consecutive peak, the STA apparatus was used rather than a tube furnace. The powder obtained by this method was spread over a flat aluminium holder and x-rayed over the angular range 25-35° at 0.02° increments, 75 seconds each. The results showed that it consisted principally of senarmontite, with some quantities of valentinite and cervantite also apparent (Fig. 5.07). Although the appearance of valentinite may indicate an unintentional overlap with the subsequent senarmontite-valentinite transition, this argument does not explain the formation of cervantite, which should be an exothermic process at this temperature. Therefore, this data appears to suggest that Peak 1 is a partial example of the polymorph phase transition, depressed by some mechanism, and possibly with related oxidation from liberated oxygen. The following peak (labelled as "P" in Figure 5.06) would then correspond to the remaining senarmontite converting to valentinite prior to melting.

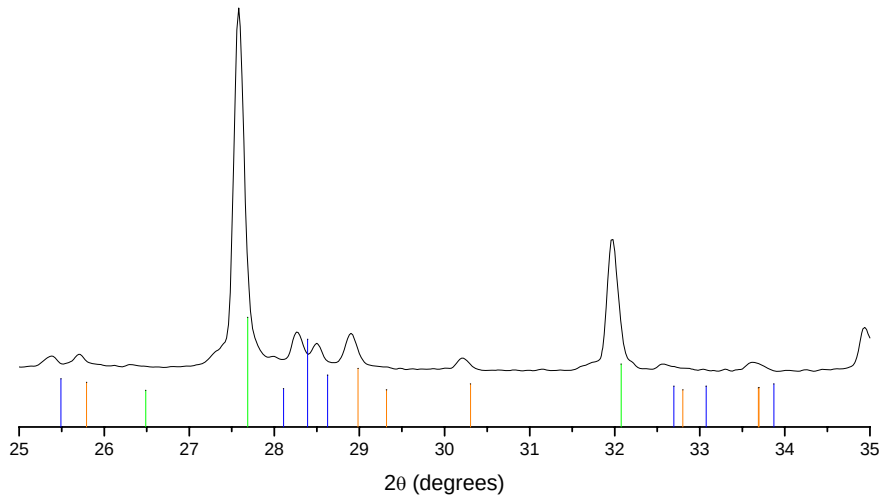

Figure 5.07 *– The XRD pattern for the commercial senarmontite heat-treated at 647°C under argon, compared with the reference peaks for senarmontite (green) [2], valentinite (blue) [3] and cervantite (orange) [1]. Due to use of the STA equipment for the thermal treatment, only a limited amount of sample was available for analysis, and the method used to mount the available powder is the likely cause of the peak shifts.*

Since the samples were all heated under argon, the cervantite formation suggests that water is chemisorbed (as hydroxyl groups) and/or physically absorbed by the Sb_2O_3, and it is the resulting liberation of this on heating that provides the oxygen necessary for oxidation. This may also be the cause of the depression of the partial phase transition – in which case, a similar effect should be observed in the water-stabilised glass samples, discussed later (Section 5.2.3). Although not immediately discernable on the heat-flow trace, the onset of "Peak P" for the milled senarmontite (at 625±3°C) suggests that a similar depressed transition may also be occurring in that sample. A white residual mass was observed in the crucibles after all STA measurements on the crystalline Sb_2O_3 samples and, although too little remained for analysis, the absence of 100% mass loss at any point on the thermogravimetric curves suggests that this is cervantite – presumably oxidised through thermal liberation of water in the samples.

The milled senarmontite also undergoes a relatively weak feature commencing at 410±5°C (labelled as "Peak 2" in Figure 5.06, and expanded for clarity). This does not correspond to any thermal event previously reported for senarmontite, so a further investigation was carried out. First, an STA scan at 20°C/min to 560°C was undertaken, which established that this feature was both repeatable and irreversible. Samples of the milled senarmontite in platinum-rhodium crucibles were then heated to 250°C and 520°C in a furnace under an argon atmosphere, and held for 4 hours before cooling. XRD analysis (Fig. 5.08) showed that the high-temperature, post-Peak 2 senarmontite produced sharper, better-defined peaks than the sample from before the thermal event.

The shape of "Peak" 2 on the STA trace and its effect on the XRD peaks suggests that it is an order-disorder transformation (reducing the stress in the substance by slight re-arrangements of bond lengths and angles) and may be related to the oxygen stoichiometry of the system, since the feature is more pronounced under flowing air (Fig. 5.09). Data for the heat-treated samples under air (Fig. 5.10) also show that, although there is some evidence of a refining of the senarmontite peaks, a small portion of the sample has also oxidised to cervantite. This is consistent with the order-disorder argument, with the atomic rearrangement providing an environment (due to short-term weakening or breaking of bonds) which allows some of the senarmontite to oxidise at a lower than normal temperature. The overall mass loss recorded over this event in the

thermogravimetric data can be explained by Sb_2O_3 volatilisation, the onset of which has been depressed for the same reasons as oxidation.

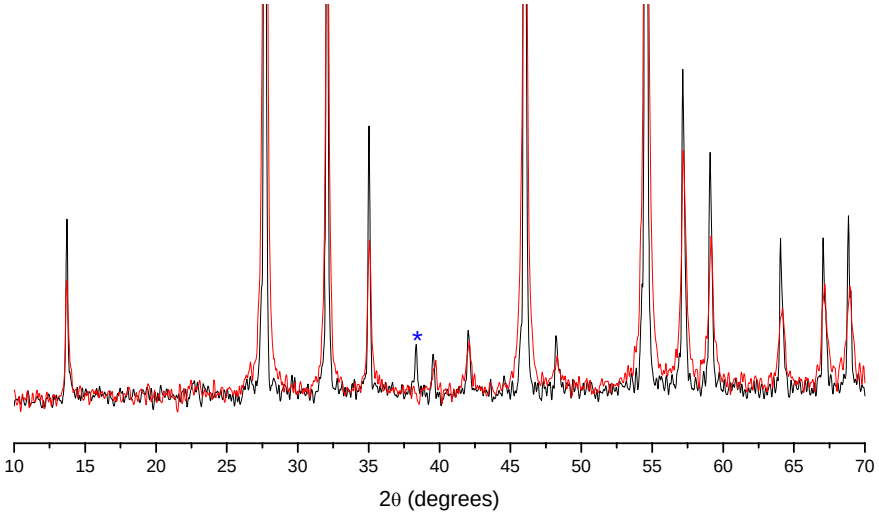

Figure 5.08 *– Comparison of the XRD traces for the milled senarmontite sample, heat-treated at 250°C (red) and 520°C (black) under argon. The starred peak is from the aluminium holder.*

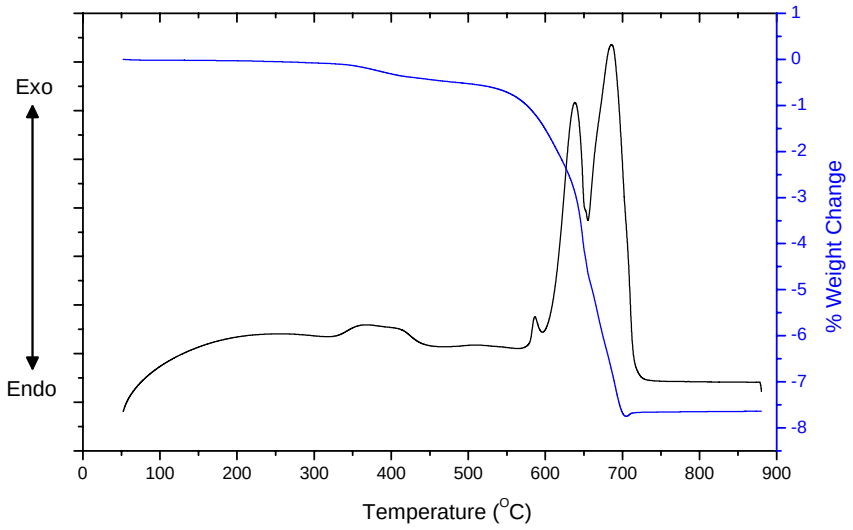

Figure 5.09 *– STA trace for the milled senarmontite sample at 40°C/min under flowing air.*

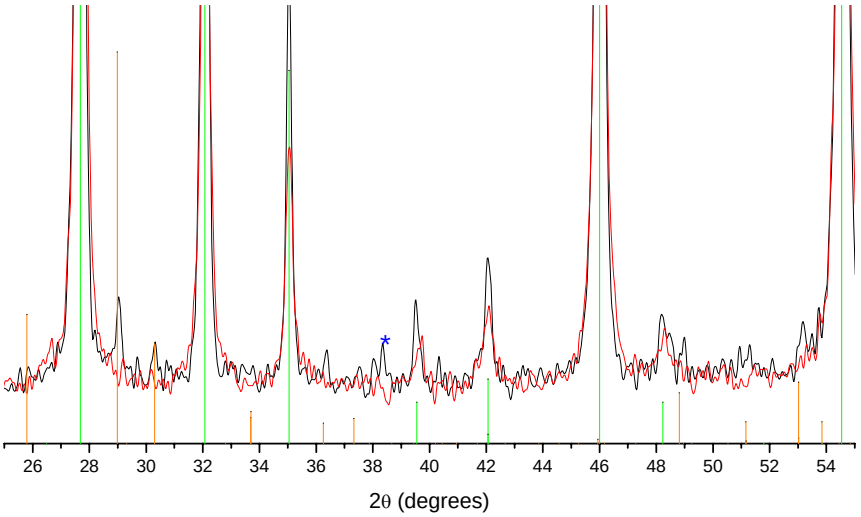

Figure 5.10 *– Comparison of the XRD traces for the milled senarmontite sample, heat-treated at 250°C (red) and 450°C (black) under air. The starred peak is from the aluminium holder. Reference peaks for senarmontite (green) [2] and cervantite (orange) [1] are also shown.*

The mechanically-derived valentinite sample also exhibited unusual behaviour in the STA measurements carried out upon it (Fig. 5.11). Although generally regarded as thermally stable below 600°C, the thermal events displayed by this sample of valentinite appear to be more consistent with those of senarmontite.

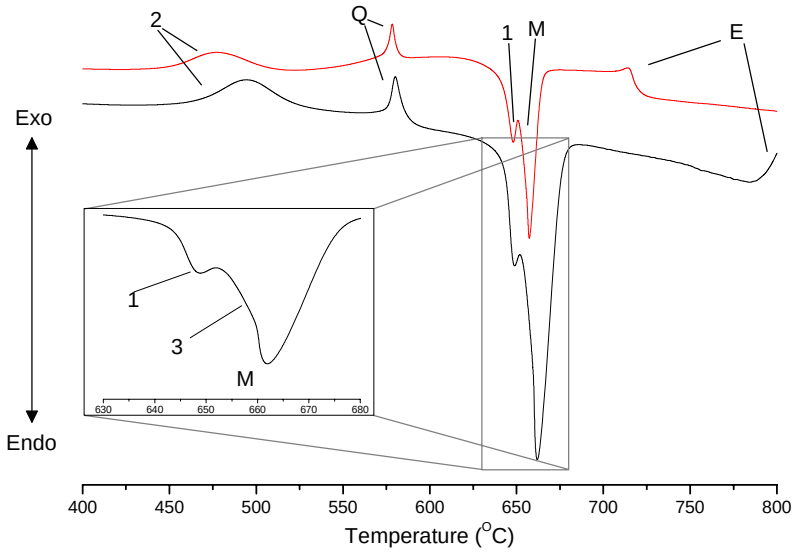

Figure 5.11 *– Comparison of the STA heat flow traces for the mechanically-derived valentinite sample under flowing argon at heating rates of 10°C/min (red) and 20°C/min (black). Peak labels: Q = α-β quartz transition; M = melting; E = end of volatilisation. Numbered peaks are discussed in more detail in the main text.*

The presence of "Peak 2", onset at 437±3°C, in the STA trace at 20°C/min – not dissimilar to the feature occurring in the milled senarmontite sample – prompted a further investigation. As earlier, a heat-treatment was carried out at a temperature above the feature (520°C) and an STA scan at 20°C/min to a maximum temperature of 560°C was undertaken to determine reversibility. This showed that the event was irreversible and XRD analysis of the resulting material revealed that the sample had completely converted to senarmontite – thus, Peak 2 arises from the valentinite-to-senarmontite transformation (this is also consistent with the exothermic nature of the feature, since the change is thermodynamically favourable at that temperature). Under argon, there was no indication of cervantite formation through oxidation, which could have provided another explanation for the event (with oxygen perhaps originating from absorbed water) – under air, Peak 2 was obscured by oxidation.

Unlike the milled senarmontite, the mechanically-derived valentinite appears to have undergone the available polymorphic transition at a lower temperature than that quoted in the literature [8]. Since no such event has previously been reported, and because there is no evidence of contamination in the XRD and Raman analysis of the sample (*q.v.* Sections 5.1.1 and 5.1.2), it seems plausible that the depression of the phase transition has occurred due to the method of sample preparation. The process of milling undertaken to produce the valentinite is likely to have produced crystallites under strain, and the additional energy present in the system as a result may have lowered the activation energy required for the transition to the thermodynamically-favourable senarmontite. Alternatively, if the process is surface-nucleated, the smaller crystallite size produced by the milling may be the cause of the lowered transition.

The presence of two endothermic peaks just before melting in the sample, as with the senarmontite samples, suggests the presence of water (the onset of the first of the peaks, at 616±3°C, matches that of the commercial senarmontite, and suggests that the pair are two-stages of the polymorphic phase transition). However, absorbed water is unlikely to be the (sole) origin of the lowered valentinite-senarmontite transition, there is no mention of this phenomenon in the literature (where, one can presume, water-containing samples are likely to have been used); it seems more plausible that the mechanical preparation of this valentinite sample, rather than a thermal one, is the primary cause.

Under air, the crystalline Sb_2O_3 samples exhibited no further unusual features beyond those already mentioned (and, indeed, those features were often partially or completely obscured by the process of oxidation; *q.v.* Section 4.3.4). As previously observed [6,9-10] oxidation of valentinite occurred at a lower temperature than in the senarmontite samples (the depressed valentinite-senarmontite transition observed in the mechanically-derived valentinite under argon was apparently overridden by oxidation under air) and an overall mass increase of 4.5% was observed. This latter contrasts with the loss of mass observed after oxidation in the senarmontite samples (again, agreeing qualitatively with the literature [6,9]) and is probably largely due to the earlier oxidation of valentinite to the stable cervantite form, preventing much of the Sb_2O_3 from volatilising. Between the senarmontite samples, overall mass loss under air was observed to be lower in the milled sample than the commercial one (2.2% versus 8.6%) – this may be due to loss of a greater amount of absorbed water in the latter, consistent with earlier arguments, or due to differing rates of volatilisation between the two Sb_2O_3 polymorphs (which could not be studied in this work due to the tendency of the mechanically-derived valentinite to convert to senarmontite if unoxidised). Under argon the reverse is true, with the milled senarmontite losing more mass, presumably due to the earlier, water-related, cervantite formation in the commercial sample.

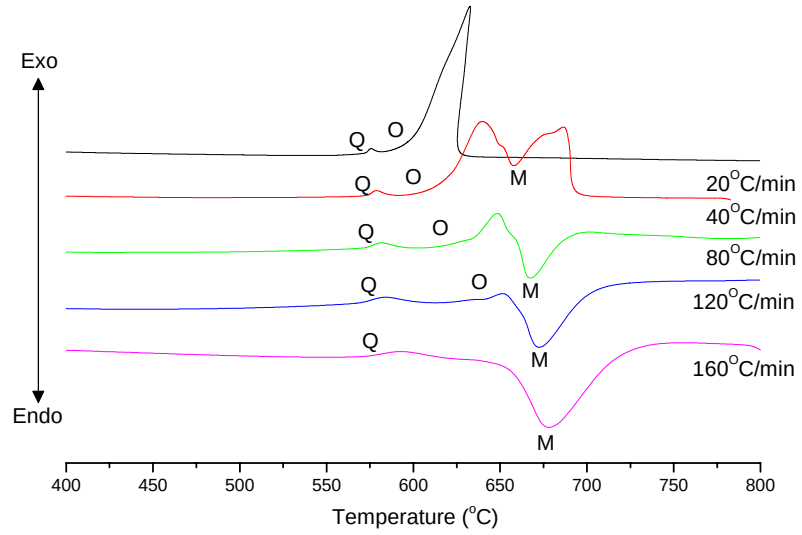

Figure 5.12 *– Comparison of the STA heat flow data for the commercial Sb_2O_3 sample at various heating rates under flowing air. The quartz α-β phase transition, oxidation onset and melting peaks are labelled (Q, O and M, respectively).*

As an aside, whilst investigating the effect of heating rate on the commercial senarmontite sample under air, it was observed that, at higher rates, melting and other

adjacent endotherms became more apparent with oxidation effectively being suppressed (Fig. 5.12). Although running at a rate high enough to eliminate oxidation rendered the fine detail of the consecutive endothermic processes indistinguishable in the samples examined here, this method could potentially be useful to access features in other oxygen-sensitive substances that would ordinarily be hidden when running under air, provided that the thermal events were well-separated.

5.1.4 Summary

The main features observed in the characterisation and thermal studies of the crystalline samples are:

- The senarmontite-valentinite transition tends to occur as a two-stage event, with the first stage apparently depressed by the presence of absorbed water in the sample.
- Mechanically-derived valentinite (produced by the method outlined by Berry and Ren [11]) converts to senarmontite at a much lower than normal temperature (437±3°C), probably due to either small crystallite size or strain in the system, as a result of the preparation by milling.
- Milled senarmontite exhibits an order-disorder transformation at 410±5°C which reduces the strain due to milling; under air, a small amount of material also oxidises to cervantite during this process.
- Some small additional peaks were observed in the cervantite XRD spectrum that are not present in the single-crystal studies.

Sample	Under Argon			Under Air	
	Senarmontite-Valentinite Phase Transition (°C ±3)	Melting Temperature (°C ±3)	Total % Mass Change	Oxidation Temperature (°C ±3)	Total % Mass Change
Commercial Senarmontite	615 (643)	652	-89.7	532	-8.6
Milled Senarmontite	625	650	-93.4	530	-2.2
Mechanically-derived Valentinite	616 (646)	654	-91.8	410	+4.6

Table 5.03 – The onset temperatures for thermal events and the mass changes in the Sb_2O_3 systems examined. Temperatures listed are for scan rates of 20°C/min except for oxidation, where onset temperatures were more easily determined from 10°C/min data. Two temperatures are given for the phase transitions where separate stages were identified (believed to be due to absorbed water). Also note that the mechanically-derived valentinite had fully converted to senarmontite prior to the events above that occur under argon.

5.2 Water-quenched Antimony Oxide Glasses

5.2.1 X-ray Diffraction and ^{1}H NMR

X-ray diffraction spectra for the two water-quenched oxide samples exhibited crystalline peaks from both polymorphs of Sb_2O_3, together with some broad, shallow features in the baseline suggesting amorphous material (Fig. 5.13). By comparison with the spectra obtained earlier for crystalline Sb_2O_3 (*q.v.* Section 5.1.1) it was possible to estimate the relative proportions of these three components.

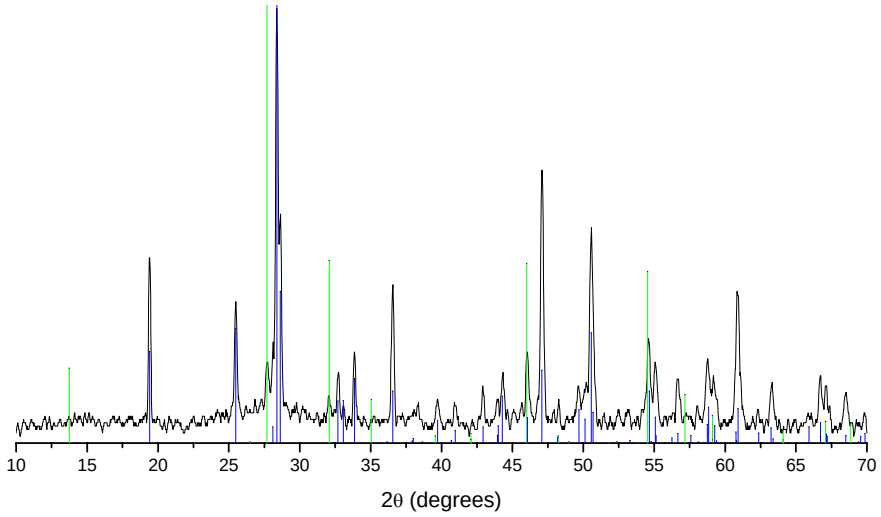

Figure 5.13 *– XRD pattern for the water-stabilised sample quenched at 850°C (also representative of the 1050°C sample) with the reference peaks for senarmontite (green) [2] and valentinite (blue) [3] also shown.*

First, an unambiguous peak of each polymorph was identified in the sample spectrum and its relative intensity in the corresponding crystalline XRD pattern was calculated by integration. The ratio of these two relative intensities was then obtained, as was the ratio of the intensities of the two chosen peaks in the sample spectrum (with the glass background subtracted). Dividing the latter by the former, the ratio of one crystalline polymorph to the other in the sample itself was obtained. Integration of the sample spectrum both with and without the glass background subtracted provided the proportion of vitreous material present (Table 5.04). These values should be treated with some caution however, since the method used makes the implicit assumptions that there is no preferred orientation in the samples and that the effect of density difference on absorption is negligible.

Sample	% Glass (±10)	% Valentinite (±5)	% Senarmontite (±1)
Sb_2O_3 water-quenched from 850°C	52	43	5
Sb_2O_3 water-quenched from 1050°C	53	44	3

Table 5.04 – Estimated compositions of the two samples.

^{1}H NMR of the 1050°C sample was undertaken using a Chemagnetics 360 NMR spectrometer at 360 MHz using a Bruker 4mm probe (static). A 1 pulse program was used with a 1s pulse delay, 1µs pulse length and 6000 acquisitions with tap water as a secondary reference at 0 ppm. The resulting spectrum after subtraction of the ^{1}H background (Fig. 5.14) shows both a broad feature indicating the presence of H_2O molecules in the sample which gives rise to a Pake doublet and a sharp peak demonstrating the presence of hydroxyl groups in the glass structure.

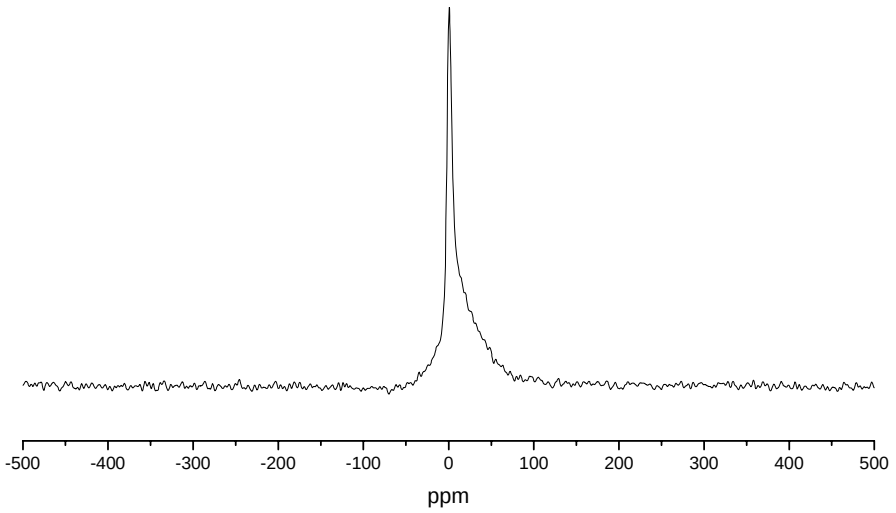

Figure 5.14 *– ^{1}H NMR spectrum for the 1050°C water-poured sample with background signal from the probe subtracted.*

5.2.2 Raman Spectroscopy

Raman spectroscopic analysis of the materials (Fig. 5.15) produced combinations of the senarmontite and valentinite peaks, supporting the XRD data; Table 5.05 lists the peaks located and their relative intensities, as compared to the crystalline polymorphs from Section 5.1.2. Only three peaks in the spectrum, at wavelength shifts of 282cm^{-1}, 339cm^{-1} and 492cm^{-1}, are not accounted for – these are some of the broader peaks, and are likely to be due to the glass content in the sample.

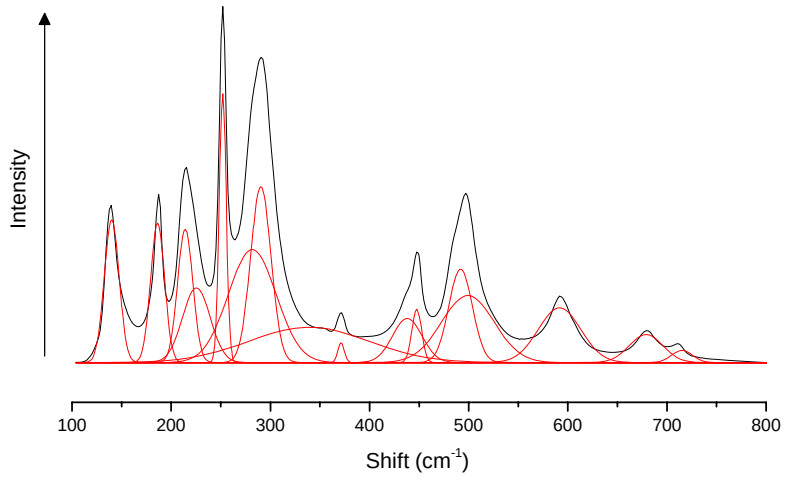

Figure 5.15 *– Peak deconvolution for the 1050°C water-quenched material (also representative of the 850°C sample).*

Water-quenched samples		**Senarmontite**		**Valentinite**	
Peak (cm^{-1} ±4)	**Rel. Intensity**	**Peak (cm^{-1})**	**Rel. Intensity**	**Peak (cm^{-1})**	**Rel. Intensity**
140	53			139	44
186	52	188	29	186	21
214	50			213	40
225	28			223	38
252	100	253	100	254	25
282	42				
290	65			291	100
339	13				
		355	1		
371	7	372	10		
438	16			440	18
448	20	450	25		
492	35				
499	25			496	55
592	20			594	19
679	10			681	8
715	5	712	4		

Table 5.05 – Comparison of the deconvoluted Raman peak values for the water-quenched samples with the peaks found for senarmontite and valentinite.

5.2.3 Thermal Analysis

The two water-stabilised "glass" samples exhibited almost identical behaviour on heating (Fig. 5.16), and their thermal events can readily be related to those of the crystalline oxides with contributions from the glass phase.

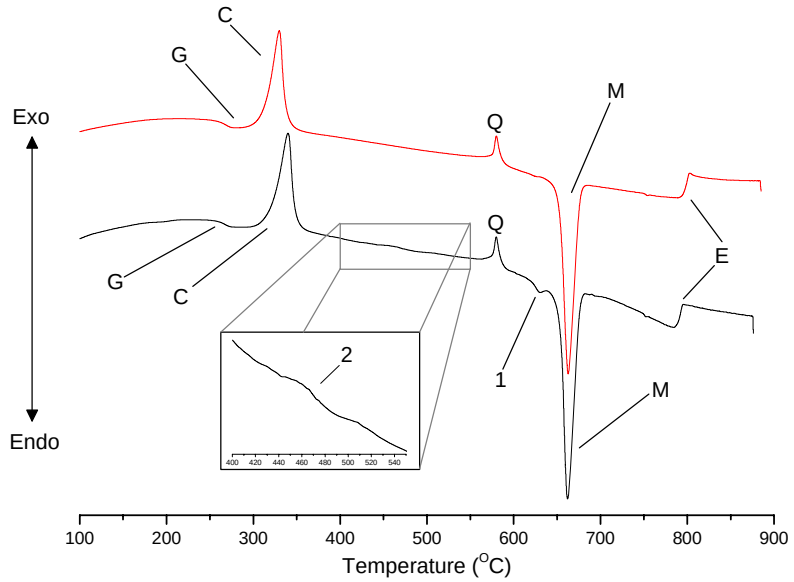

Figure 5.16 *– Comparison of the heat flow curves from the 20°C/min STA runs under argon for the 850°C (red) and 1050°C (black) water-poured glasses. Peak labels: G = glass transition; C = crystallisation; Q = α-β quartz transition; M = melting; E = end of volatilisation. Numbered peaks are discussed in more detail in the main text.*

The absence of an obvious senarmontite-to-valentinite transition very close to melting was unexpected, given the existence of small amounts of the former in the original sample (*q.v.* Section 5.2.1), although "Peak 1" bears similarities to the depressed phase transition observed in the crystalline Sb_2O_3 samples. In order to determine the composition post-crystallisation of the glass, a heat-treatment was carried out on each of the samples at 390°C for 4 hours under a flowing argon atmosphere. XRD analysis of the resulting materials identified the presence of both phases of Sb_2O_3, and their relative proportions were calculated by integration for comparison with the values obtained in Section 5.2.1 for the crystalline portions of the glass samples (and using the method outlined in that section). The calculated values are given in Table 5.06 and show that approximately 75% of the glass crystallises to senarmontite, with the remainder forming valentinite.

Sample	**% Valentinite**		**% Senarmontite**	
	Original Crystalline Material (±5)	**Post-glass Crystallisation (±4)**	**Original Crystalline Material (±1)**	**Post-glass Crystallisation (±4)**
Sb_2O_3 water-quenched from 850°C	43	59	5	41
Sb_2O_3 water-quenched from 1050°C	44	55	3	45

Table 5.06 – Estimated compositions of the crystalline portion of the two samples, before and after the glass crystallisation event.

This suggests that a senarmontite-valentinite phase transition should indeed be present. Close examination of the thermal trace for the 1050°C sample between crystallisation and the α-β transition of the quartz reference revealed a small feature (Peak 2) occurring over the range (419-506)±3°C. A further heat-treatment of the original preparation of this material was undertaken at 510°C under flowing argon for 4 hours, and the resulting powder was examined using XRD (Fig. 5.17).

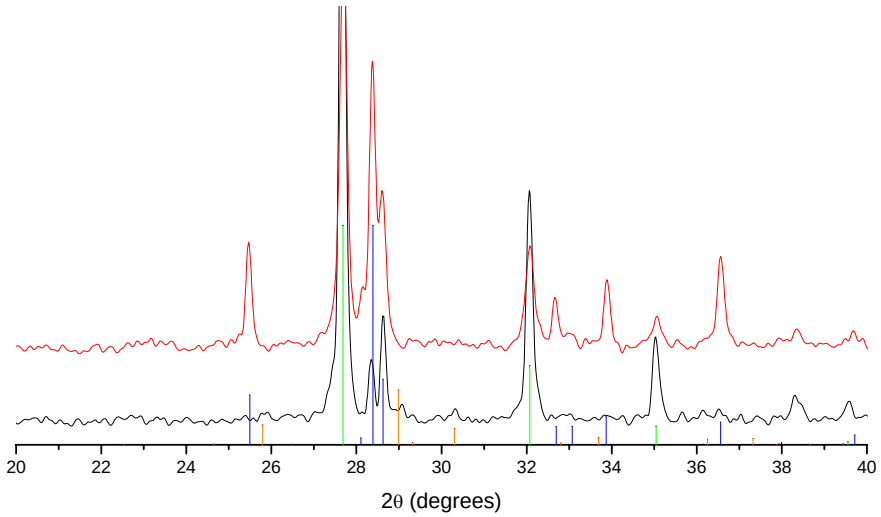

Figure 5.17 *– Comparison of the XRD traces for the 1050°C water-poured sample just after crystallisation at 390°C (red) and after Peak 2 at 510°C (black) under argon. Also shown are the reference peaks for senarmontite (green) [2], valentinite (blue) [3] and cervantite (orange) [1].*

Analysis of the XRD trace shows that the valentinite portion of the sample has been significantly reduced, and the senarmontite correspondingly increased. There also appears to be a small amount of cervantite present in the sample at this point. As with the mechanically-derived sample examined earlier, it appears that the valentinite formed in the water-poured materials is inclined to undergo the conversion to senarmontite at a lower than normal temperature. The formation of small amounts of cervantite is also interesting: it suggests that water is being liberated in the process and is oxidising a portion of the valentinite (the temperature is too low for senarmontite oxidation). Although these samples have not been milled like the other, it is possible that either the original crystalline material or the glass in crystallising may have formed valentinite with such a large amount of absorbed water that the structure of the

crystallites is under strain, thus lowering the activation energy required for the phase transition to occur.

The only remaining thermal event which the sample undergoes before melting is a small endothermic feature (labelled as Peak 1 in Figure 5.16), onset temperature of 615±3°C. Another heat-treatment of the original 1050°C sample was conducted at 637°C for 3 minutes under flowing argon, and the product analysed as before. To achieve the necessary accuracy for this thermal treatment – to avoid the onset of melting – the process was conducted using the STA apparatus, and the resulting powder x-rayed (Fig. 5.18), in the manner described earlier (*q.v.* Section 5.1.3).

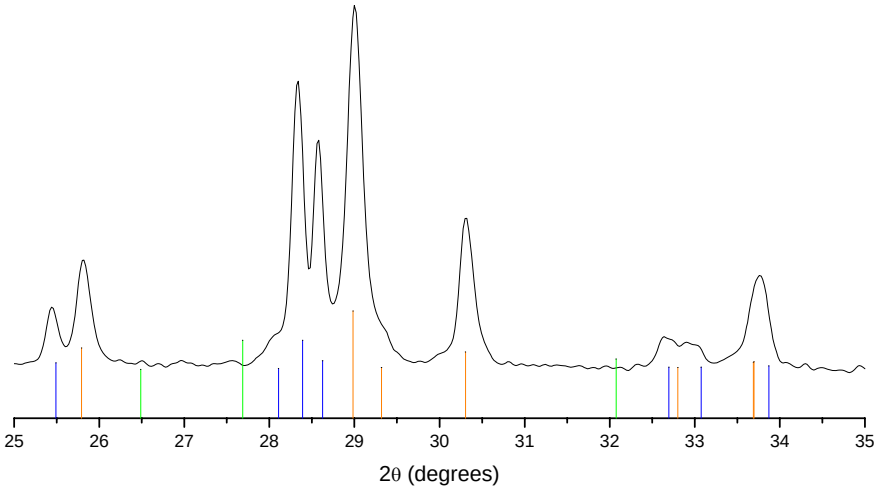

Figure 5.18 *– XRD trace of the 1050°C sample after heat-treatment at 637°C, overlaid with the reference peaks for senarmontite (green) [2], valentinite (blue) [3] and cervantite (orange) [1].*

The XRD data reveals that, following Peak 1, all of the senarmontite in the sample has converted to valentinite, whilst the amount of cervantite present has also increased. Thus it appears that Peak 1 corresponds to the senarmontite-valentinite phase transition, depressed to a lower than normal temperature.

The depression of the phase transition in the water-poured samples further reinforces the conclusions drawn for the crystalline Sb_2O_3 samples, namely that it is caused by absorbed water. The increased oxidation and total nature of the depressed transition (compared with the two-stage transition observed in the crystalline samples) is consistent with the greater amount of water likely to be bound up in the water-poured samples.

Under air, it is apparent that oxidation is a two-stage process (Fig. 5.19) with the process commencing at 462±5°C (453±5°C for the 850°C sample) and experiencing a sharp change in slope at 511±5°C. These would appear to conform approximately with the oxidation of the valentinite and the senarmontite in the samples, respectively, although the onset temperatures do not match those observed for the crystalline samples (*q.v.* Section 5.1.3). Consistent with the large proportion of valentinite in the sample, the overall mass change for the samples is slightly positive (1% overall mass gain) after oxidation, but lower than for a pure valentinite sample. Examination of the thermogravimetric curves also shows that mass loss begins to occur at a significant rate earlier than in the crystalline samples, probably due to the loss of water that has been adsorbed; this has likely also contributed to the lower overall gain in mass compared with pure (and drier) valentinite.

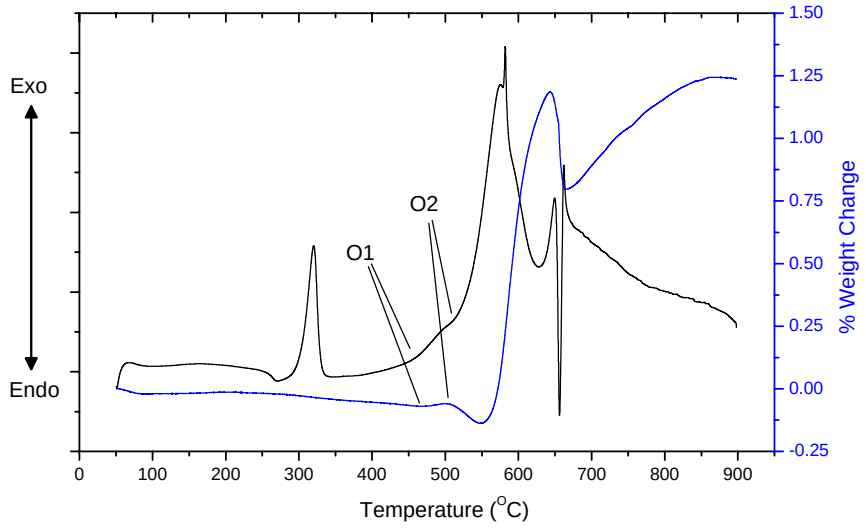

Figure 5.19 *– STA data for the 850°C sample under flowing air at a heating rate of 10°C/min. O1 and O2 mark the onsets of the first and second stages of oxidation, respectively.*

As described in Section 4.3.3 (*q.v.*) DSC measurements were used to obtain Kissinger plots for each of the water-stabilised samples (Fig. 5.20). The activation energies of crystallisation obtained are given in Table 5.07. The difference in values requires further investigation.

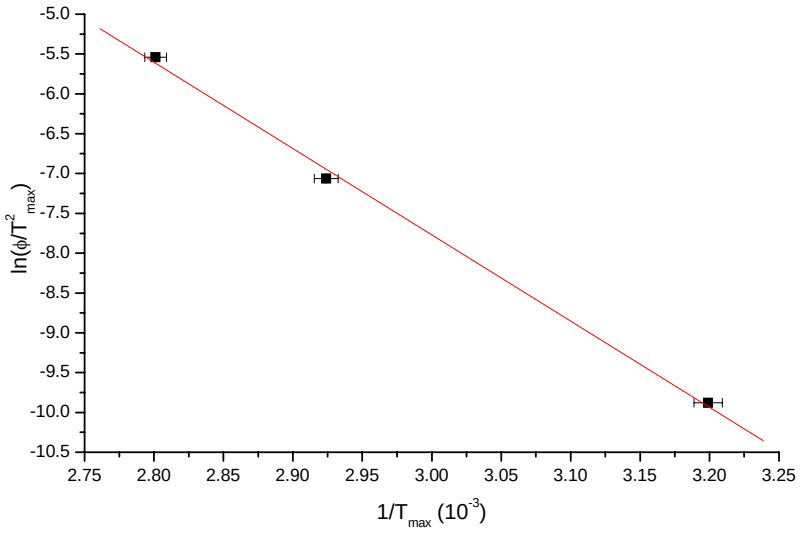

Figure 5.20 *– Kissinger plot for the 1050°C water-stabilised sample, calculated from DSC data.*

Sample	Crystallisation Activation Energy (kJ/mol ± 6.4)
850C	69.4
1050C	89.8

Table 5.07 – Crystallisation activation energies calculated from the Kissinger plots for the water-stabilised samples.

5.2.4 Summary

The principal observations from the characterisation and thermal studies of the water-quenched samples are:

- The samples obtained consist of approximately 52% vitreous material, with the remaining crystalline content consisting primarily of valentinite. Upon crystallisation, the glassy material forms senarmontite and valentinite in a 3:1 ratio.
- Post-crystallisation, the majority of the valentinite in the sample undergoes a depressed phase transition to senarmontite (as with the mechanically-derived valentinite examine earlier), probably due to having formed under strain (either on quenching or upon crystallisation of the glass) due to the high water content.
- The senarmontite-valentinite transition is also depressed, also as per the crystalline samples, although now the entire transformation occurs in a single stage. This is likely due to a combination of the effects of greater water content

in the sample and the possible formation of strained senarmontite during glass crystallisation.

Sample	Under Argon*					Under Air	
	T_g (°C ±5)	T_c (°C ±5)	Senarmontite-Valentinite Phase Transition (°C ±5)	Melting Temperature (°C ±5)	Total % Mass Change	Oxidation Temperature** (°C ±5)	Total % Mass Change
850°C water-poured glass	255	310	617	639	-92.8	453 (511)	+1.0
1050°C water-poured glass	256	316	615	641	-94.0	462 (511)	+1.0

Table 5.08 – Temperatures of thermal events and the mass changes in the water-stabilised glass systems investigated. Temperatures listed are from 20°C/min STA scans except for oxidation, where onset temperatures were more easily determined from 10°C/min data.
* The glass transition and crystallisation temperatures showed no variation with atmosphere (melting onset temperature could not be measured with accuracy under air due to oxidation).
** Since oxidation appears to be a two-stage process in these samples (as discussed in the main text) onset temperatures are given for each stage.

5.3 Chlorine-stabilised Antimony Oxide Glasses

5.3.1 Sample Appearance

The glasses formed by the method outlined in Section 4.1.5 (Fig. 5.21) were a pale yellow in colour, approximately 1mm thick and translucent with some evidence of deposits (presumably chlorine-rich) on or near the surface. There was evidence of phase separation within the x = 0.85 preparations, with the majority (95% or greater) forming a material akin to that already described, whilst the remaining minority cooled to leave a much paler glass with no visible evidence of surface deposits.

Figure 5.21 *– An example of the chlorine-stabilised glass produced (the October '04 50/50 sample).*

5.3.2 X-ray Diffraction

XRD scans of the chlorine-stabilised glasses gave purely vitreous signals for the 50/50 glasses and the "g" phases of the 85/15 samples (Fig. 5.22), whilst the 70/30 glasses and the "c" phases of the 85/15 samples returned mixed vitreous and crystalline spectra (Fig. 5.23). The latter portion matched reference patterns for onoratoite ($Sb_8O_{11}Cl_2$) and valentinite (Fig. 5.24).

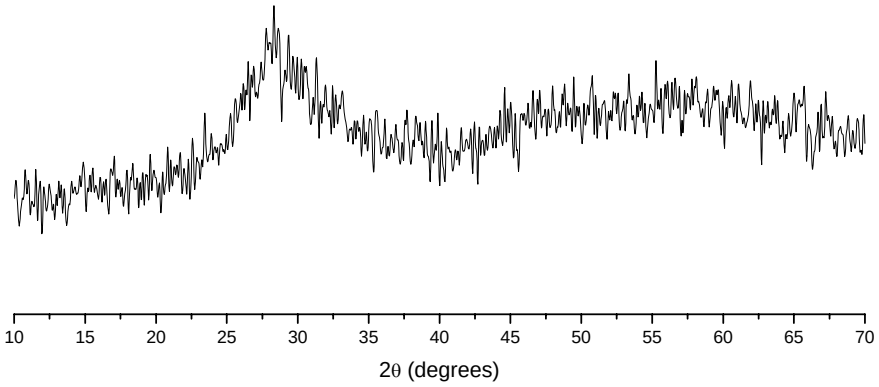

Figure 5.22 *– XRD pattern representative of the purely vitreous chlorine-stabilised glasses.*

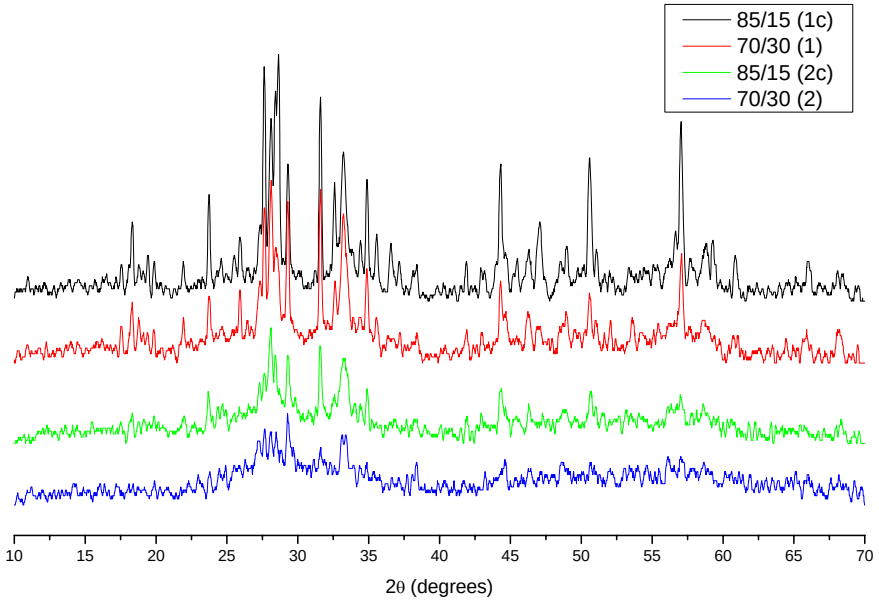

Figure 5.23 *– Comparison of the XRD spectra obtained for the mixed crystalline/vitreous samples; it is evident that the same crystalline phases are present in all four, and that the proportion of crystalline material present appears to decrease as the initial chlorine content increases. The differences in the two methods of preparation also appear to have been significant.*

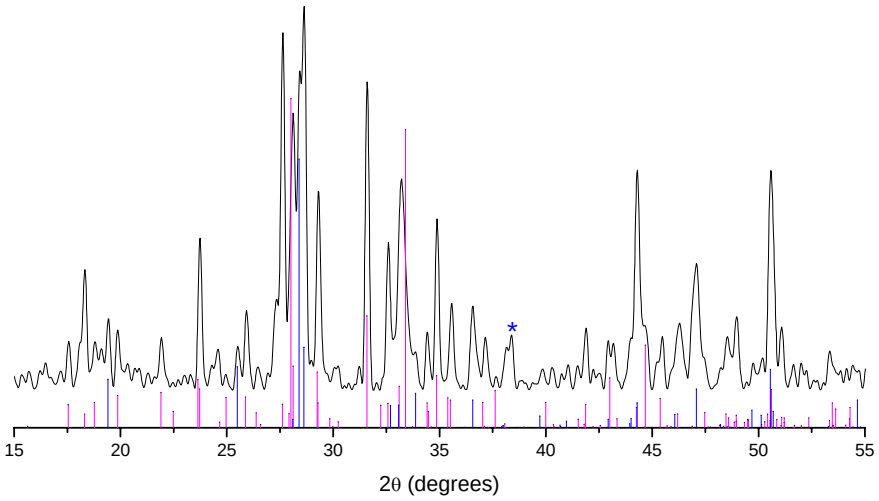

Figure 5.24 *– Comparison of the XRD pattern for the 85/15 (1c) sample (representative of the other mixed crystalline/vitreous spectra and with the glass background subtracted) with the reference peak positions for valentinite (blue) [3] and onoratoite (magenta) [4]. The starred peak is from the aluminium sample holder.*

5.3.3 Energy Dispersive X-ray Analysis

EDX analysis of the samples in their powdered form was undertaken to obtain estimates of their chlorine content (the results are listed in Table 5.12 in Section 5.3.7). Scanning Electron Microscopy (SEM) images were also obtained of the surfaces of sample fragments (Fig. 5.25).

In the SEM images, there appeared to be evidence of surface crystallisation on the 70/30 (1) sample, and a fragment was analysed using 'glancing angle' XRD (θ fixed at 3°, with only the detector changing angle) over an angular range of 20-55° at 0.02° increments, 60 seconds collection time per increment. The results show that the surface crystallisation comprises valentinite, onoratoite and senarmontite (Fig. 5.26). The absence of the latter from the XRD analysis of the powdered material suggests that this senarmontite formation is only present at the surface. This may be due to differences in nucleation and crystallisation processes on the surface as opposed to those for the bulk material during cooling of the melt.

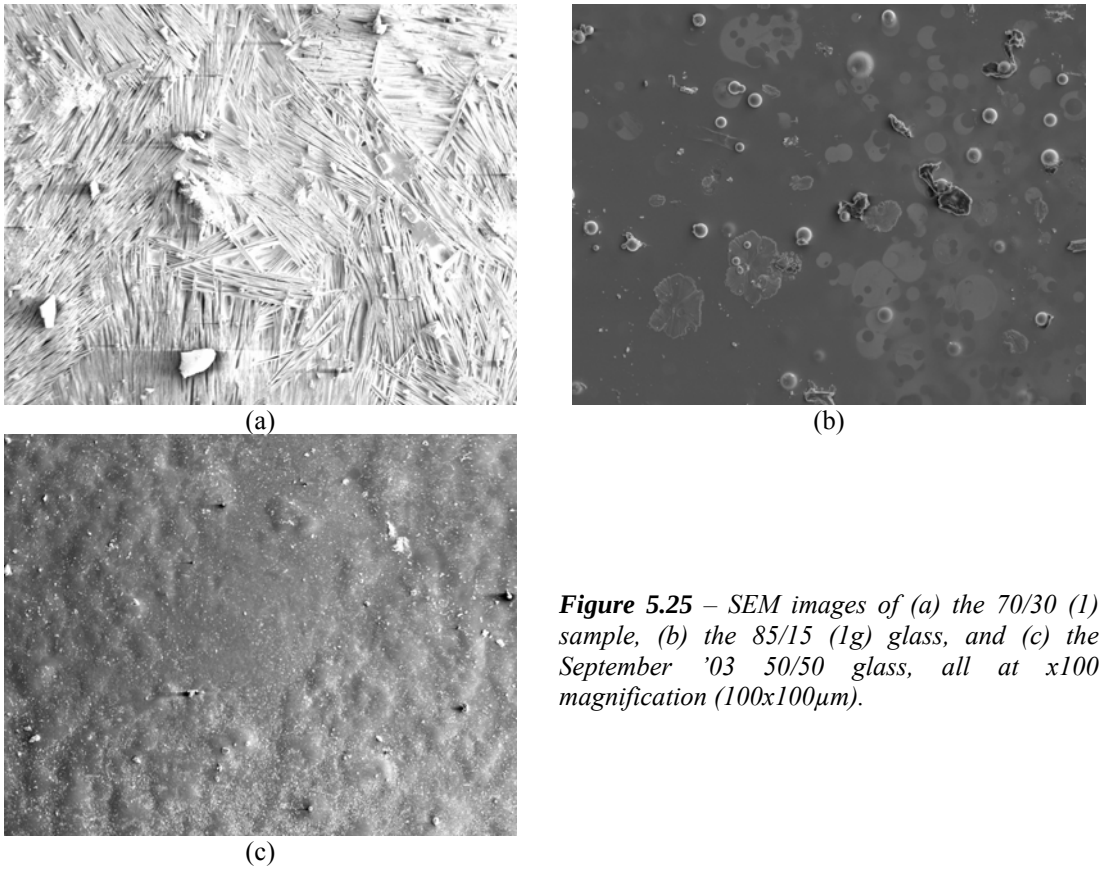

Figure 5.25 *– SEM images of (a) the 70/30 (1) sample, (b) the 85/15 (1g) glass, and (c) the September '03 50/50 glass, all at x100 magnification (100x100µm).*

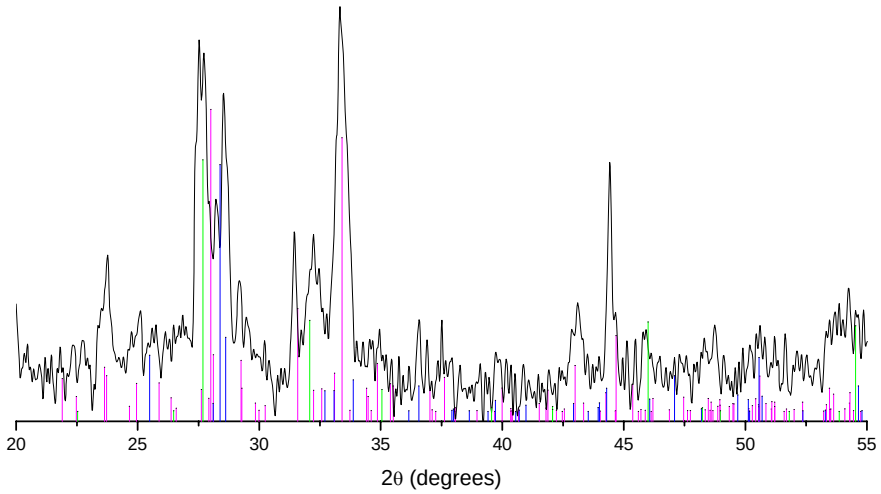

Figure 5.26 *– XRD pattern obtained for a fragment of the 70/30 (1) sample using the 'glancing angle' technique. Reference peaks for senarmontite (green) [2], valentinite (blue) [3] and onoratoite (magenta) [4] are also shown.*

5.3.4 Raman Spectroscopy

Raman spectra for the chlorine-stabilised samples supported the (qualitative) identification of amorphous and crystalline contents in the samples determined by

XRD, with partially crystalline samples exhibiting a greater number of, and better-defined, peaks than the purely amorphous samples (Figs. 5.27 and 5.28).

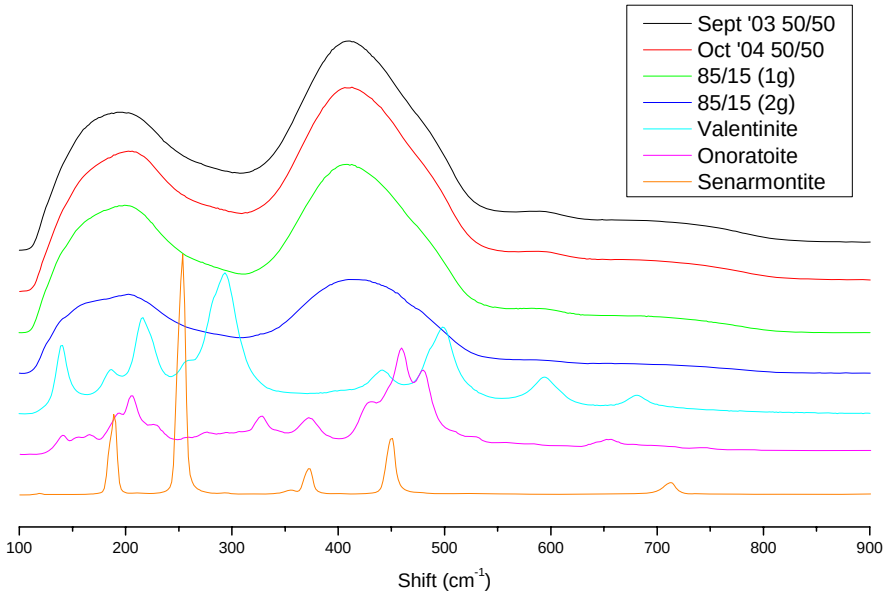

Figure 5.27 *– Raman spectra of the samples identified by XRD as being purely amorphous, compared with the Raman spectra for the crystalline oxides.*

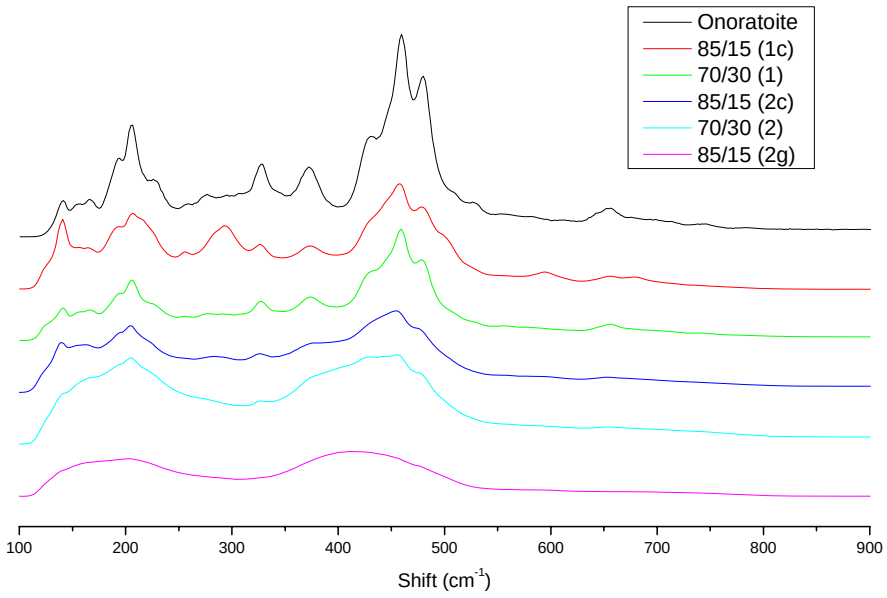

Figure 5.28 *– Raman spectra of the chlorine-stabilised samples identified by XRD as being a mixture of amorphous and crystalline material, with the spectra of the crystalline onoratoite and 85/15 (2g) samples provided for comparison.*

It is apparent from the Raman spectra and intensities that, qualitatively, the glass samples produce a similar distribution of Raman shifts to crystalline onoratoite (this is clearest in Figure 5.28, where crystalline content decreases down the plot) suggesting that the basic structure of the glass is similar to it, rather than senarmontite or valentinite. The expected chlorine content of onoratoite (9.5 at.%) is also similar to that measured by EDX in the glass samples, within estimated error (*q.v.* Table 5.12 in Section 5.3.7).

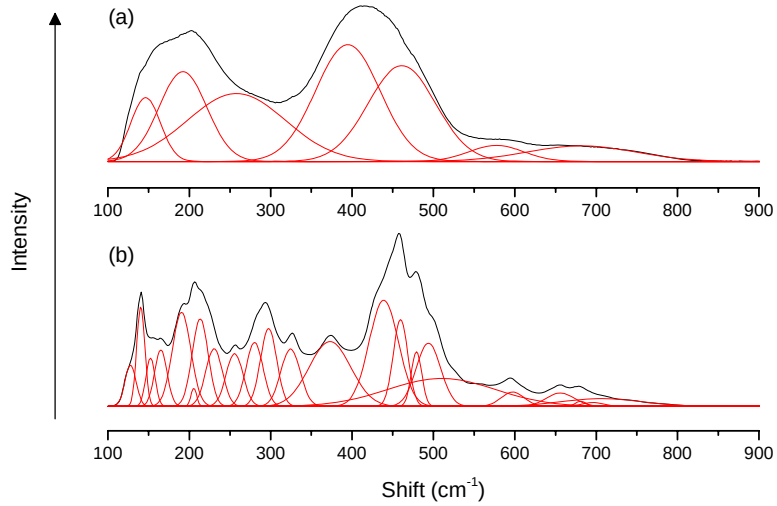

Figure 5.29 *– Raman spectra for (a) the 85/15 (2g), and (b) the 85/15 (1c) samples (representative of all of the fully amorphous and mixed crystalline/amorphous samples, respectively).*

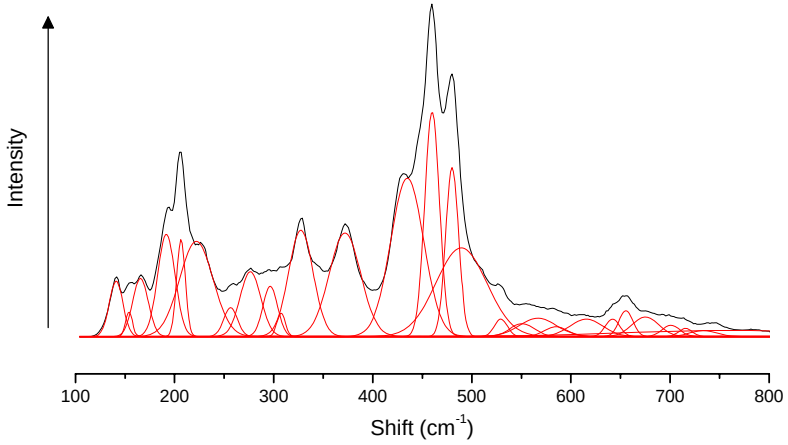

Figure 5.30 *– Raman spectrum for the crystalline onoratoite sample, with peaks deconvoluted.*

85/15 (2g)		85/15 (1c)		Onoratoite	
Peak (cm^{-1} ±4)	Rel. Intensity	Peak (cm^{-1} ±4)	Rel. Intensity	Peak (cm^{-1} ±4)	Rel. Intensity
		128	39		
		140	94	141	25
146	55				
		152	46	154	11
		165	53	166	26
192	77	191	89	192	46
		206	17	206	43
		213	83		
				222	42
		230	54		
258	58	256	50	257	13
		280	60	276	29
		297	74	297	22
				307	11
		324	54	327	47
		373	61	372	46
395	100				
		439	100	435	70
461	82	460	82	460	100
		479	52	480	75
		494	60	489	40
		510	26		
				529	8
				551	6
				567	8
577	14				
				585	4
		597	13		
				616	8
				642	8
		656	13	656	12
				675	9
682	13	681	5	680	<1
		696	4	701	5
		707	7	716	4
				734	3
				757	3

Table 5.09 – Deconvoluted peak positions and relative intensities for the Raman spectra plotted in Figures 5.29 and 5.30, compared with onoratoite.

5.3.5 Water-treatment

To determine whether or not the chlorine-stabilised glasses were sensitive to water, a powdered specimen of the Oct ’04 50/50 glass was submerged in an excess of cold water for 2 hours, placed in an oven at 80°C for 20 hours to dry, and examined using x-ray diffraction and Raman spectroscopy.

XRD revealed that the sample had undergone significant crystallisation, although some vitreous material was still present (each crystallite is likely to have formed a crystalline layer around a glassy core, not dissimilar to the macroscopic

situation a glass fragment would undergo), and the resulting peaks matched those of valentinite (Fig. 5.31). Raman spectroscopy identified no further components in the sample (Table 5.10), where the five peaks not corresponding to valentinite are probably due to the glass remaining in the sample.

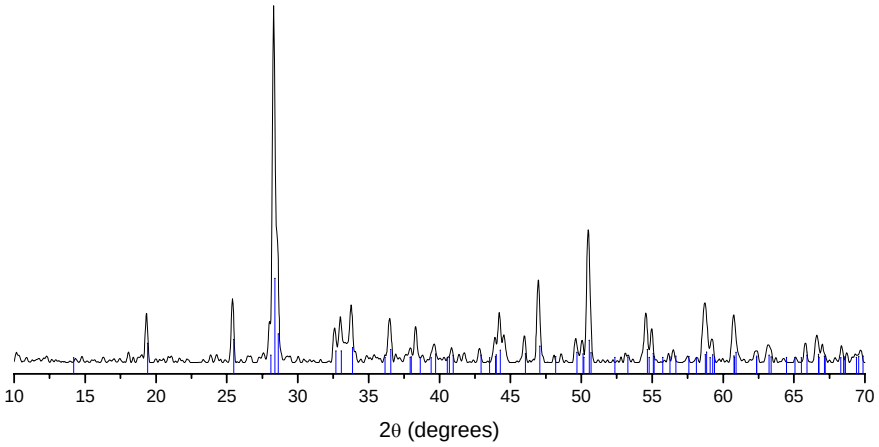

Figure 5.31 *– The XRD pattern for the water-treated sample (glass background subtracted) compared with the reference peaks for valentinite (blue) [3].*

Water-treated Oct '04 50/50 glass		**Valentinite**	
Peak (cm^{-1} ±4)	**Rel. Intensity**	**Peak (cm^{-1} ±4)**	**Rel. Intensity**
140	46	139	44
159	17		
188	32	186	21
215	54	213	40
226	26	223	38
259	24	254	25
278	8		
293	100	291	100
313	25		
442	38	440	18
487	26		
501	40	496	55
509	25		
594	29	594	19
678	12	681	8

Table 5.10 – Raman peaks identified by deconvolution in the water-treated chlorine-stabilised glass sample.

The crystallisation products of the samples due to reaction with atmospheric moisture (see photo Fig. 5.25a) are likely to be different to those of the samples immersed in water, where any chlorine leached from the material by the water is removed from the interface. It is apparent from the planar nature of the crystal structures of onoratoite and valentinite (Figs. 5.32a and 5.32b, respectively) that both are suited to insertion of chlorine between planes, more so than senarmontite (Fig. 5.32c).

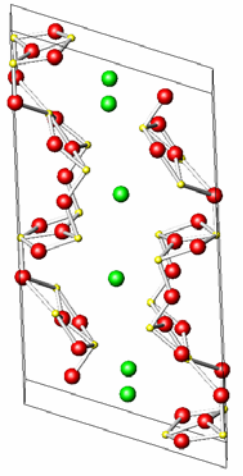

(a)

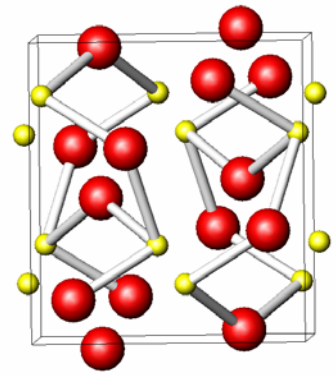

(b)

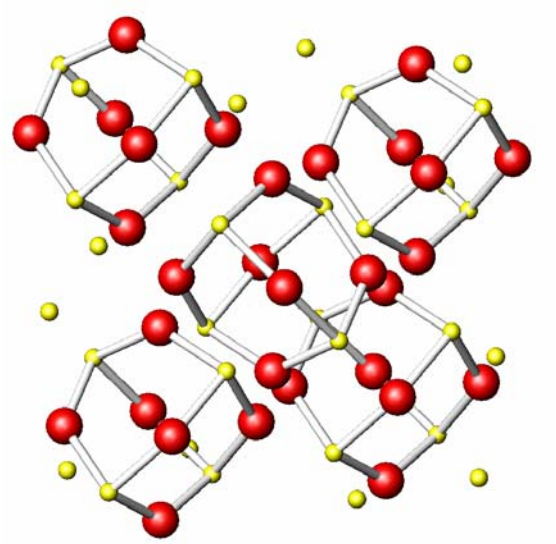

(c)

Figure 5.32 *– Crystal structures of (a) onoratoite, (b) valentinite, and (c) senarmontite.*

5.3.6 Thermal Analysis

Thermal analysis of the chlorine-stabilised glasses revealed several unexpected features. Many of the samples exhibited what appeared to be two glass transition events, which could have implied a degree of phase separation, but the absence of this feature in the thermal data from a glass fragment (Fig. 5.33) instead suggests a sintering process occurring prior to crystallisation of the devitrified glass. The crystallisation process itself is probably surface-nucleated, and thus begins earlier in the powder than in the fragment.

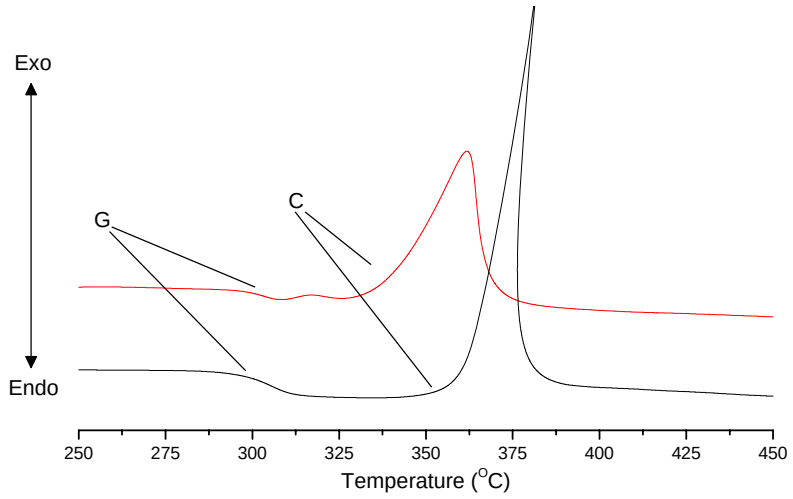

Figure 5.33 *– Comparison of the DTA component of the 20°C/min STA scans of powdered 70/30 (2) glass (red) and a whole fragment of the same sample (black) under argon.*

To determine the crystallisation products of the glass systems, samples of the (initially) purely vitreous and partially crystallised samples (specifically, the Oct. '04 50/50 and 85/15 (2c) samples) were heat-treated at 390°C under argon for four hours. The resulting materials were subjected to XRD analysis, and these results showed that both glasses had crystallised to a mixture of senarmontite and onoratoite, with some valentinite (Fig. 5.34).

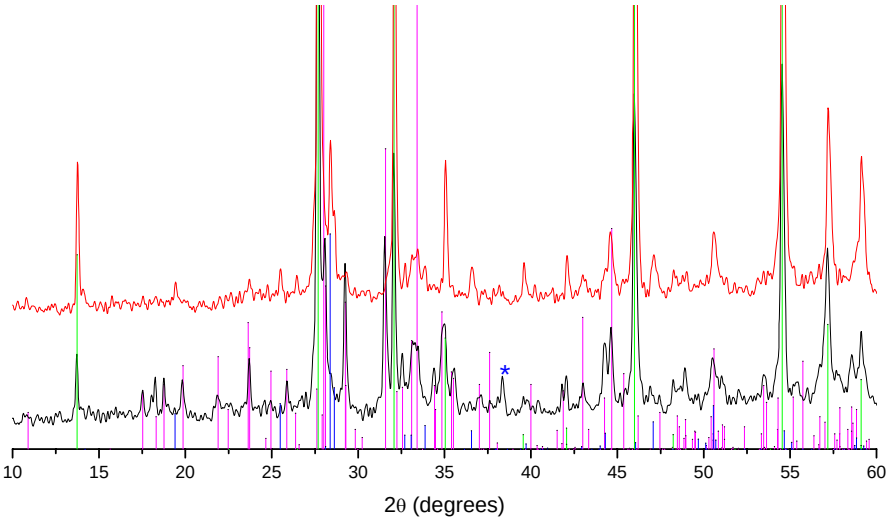

Figure 5.34 *– XRD patterns obtained from samples heat-treated at 390°C for the 85/15 (2c) sample (black) and the October '04 50/50 glass (red). Reference peaks for senarmontite (green) [2], valentinite (blue) [3] and onoratoite (magenta) [4] are also shown. Some of the more intense senarmontite peaks have been truncated; the starred peak is from the aluminium holder.*

STA data for the chlorine-stabilised samples (Fig. 5.35) show a small feature in the heat-flow curve, onset at 408±3°C, which is reminiscent of the depressed

valentinite-senarmontite event observed in the water-poured samples. A heat-treatment was carried out on a sample of the October '04 50/50 glass at 510°C for 4 hours under flowing argon, and the resulting powder was analysed with XRD to determine the sample composition following this feature (Fig. 5.36).

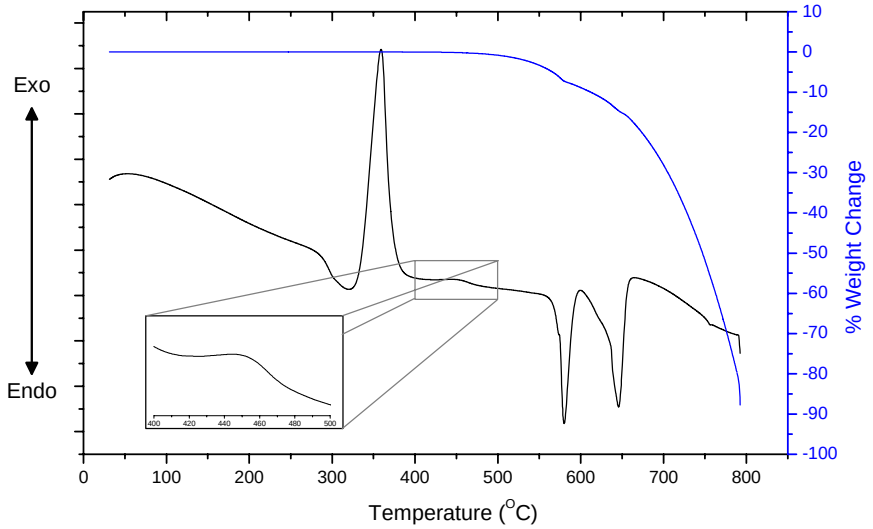

Figure 5.35 *– STA trace for the October '04 50/50 glass at a heating rate of 20°C/min under argon. The trace is representative of all the chlorine-stabilised samples.*

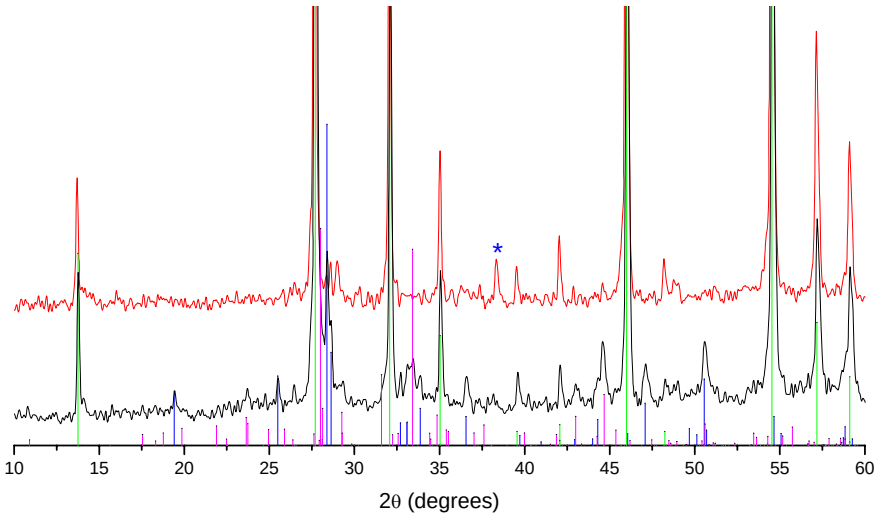

Figure 5.36 *– Comparison of the XRD patterns obtained for the October '04 50/50 glass after crystallisation at 390°C (black) and at 510°C (red). Reference peaks for senarmontite (green) [2], valentinite (blue) [3] and onoratoite (magenta) [4] are also shown. Some of the more intense senarmontite peaks have been truncated; the starred peak is from the aluminium holder.*

The comparison of the pre- and post-event XRD spectra clearly show that the valentinite in the sample appears to have been fully converted to senarmontite – as was observed in earlier samples – and the onoratoite content has also significantly decreased. Whilst the former event appears to suggest that the crystallised valentinite has formed under strain – possibly due to the presence of chlorine rather than water – the decrease in onoratoite content may be related to the endothermic event that occurs next in the system (discussed below), where the furnace used for the heat-treatment may have slightly overshot the mark.

The remaining endothermic events occurring in the heat-flow trace bear a noticeable similarity to those of the crystalline onoratoite under the same conditions (Fig. 5.37). In particular, the first event ("Peak 1") corresponding to the thermal decomposition of onoratoite to senarmontite and $SbCl_3$ (the latter escaping as a gas, with associated mass loss in the sample), which further suggests that the elimination of onoratoite suggested in the 510°C heat-treatment above may be doubtful.

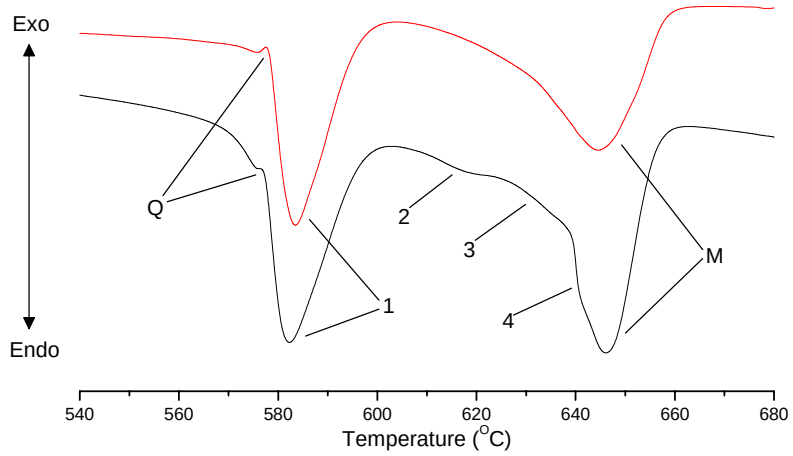

Figure 5.37 *– A section of the STA heat flow trace at 20°C/min under argon for the 85/15 (1g) sample (black) and the crystalline onoratoite (red). Peak labels: Q = α-β quartz transition; M = melting. Numbered peaks are discussed in more detail in the main text.*

The three peaks remaining before melting also appear to be present in the thermal behaviour of the crystalline onoratoite, although they are better defined when obtained from the initially vitreous sample. The exact nature of these peaks has not been determined, due to the difficulties involved in heat-treating samples accurately without overrun into adjacent events. However, based on the work in earlier sections, it can be hypothesised that the three events correspond to the senarmontite-valentinite

transition occurring in multiple stages before melting – conversion of material strained due to glass crystallisation, followed by that of senarmontite strained from formation during onoratoite decomposition, and finally that of unstrained material formed from the earlier valentinite-senarmontite transition, perhaps.

DSC measurements of crystallisation in the chlorine-stabilised samples were used to calculate values for Kissinger plots (Fig. 5.38). The activation energies calculated from these plots are given in Table 5.11; it is apparent from the values obtained that there appears to be a decrease in the activation energy required with the age of the sample in the 50/50 glasses – this effect may be due to the introduction of hydroxyl groups.

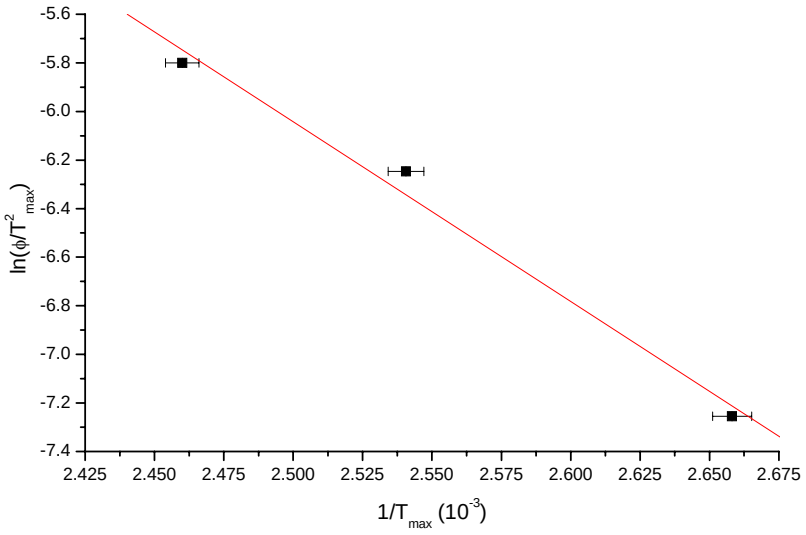

Figure 5.38 *– Kissinger plot for the December-powdered October '04 50/50 chlorine-stabilised sample, calculated from DSC data.*

Sample	Crystallisation Activation Energy (kJ/mol ±6.4)
85/15 (1g)	63.5
85/15 (1c)	–*
85/15 (2g)	–*
85/15 (2c)	65.6
70/30 (1)	48.8
70/30 (2)	61.7
Sept. '03 50/50	35.1
Oct. '04 50/50	47.9
December-powdered Oct. '04 50/50	61.8

Table 5.11 – Crystallisation activation energies calculated from the Kissinger plots for the chlorine-stabilised samples.
* Peak measurements for these samples were not possible due to a lack of resolution in the DSC data.

5.3.7 Summary

Sample	at.% Chlorine* (±2.0)	Under Argon**			Under Air	
		T_g (°C ±3)	T_c (°C ±3)	Total % Mass Change	Oxidation Temperature (°C ±5)	Total % Mass Change
85/15 (1g)	7.5	296	333	-95.6	510	-9.1
85/15 (1c)	7.9	296	333	-90.6	505	-9.0
85/15 (2g)	8.2	298	331	-89.6	–***	–***
85/15 (2c)	8.3	295	334	-96.9	507	-11.4
70/30 (1)	8.2	299	332	-94.8	509	-8.6
70/30 (2)	10.5	297	334	-92.4	508	-12.6
Sept. '03 50/50	6.0	285	337	-92.2	502	-4.9
Oct. '04 50/50	6.9	286	331	-92.9	494	-6.9
Dec.-powdered Oct. '04 50/50	6.6	286	332	-93.8	503	-9.4

Table 5.12 – Temperatures of the thermal events and the mass changes in the chlorine-stabilised glass systems investigated. Temperatures listed are all from 20°C/min STA scans – in particular this means that the oxidation values should be reduced by ~20°C for a meaningful comparison with the values given in Table 5.03.
* Determined from the EDX measurements of powdered samples (*q.v.* Section 5.3.3).
** The glass transition and crystallisation temperatures showed no variation with atmosphere.
*** The 85/15 (2g) glass was not run under air due to the limited amount of sample available.

The main points to note from the characterisation and thermal studies of the chlorine-stabilised samples are:

- The 70/30 and 85/15 glasses formed materials with both vitreous and crystalline portions on quenching of the melt. The crystalline phase consisted of valentinite and onoratoite, with a small amount of senarmontite detectable at the surface in some cases. The 50/50 preparations produced purely glassy material.
- Raman data suggests that the glasses have a structure similar to that of onoratoite.
- After immersion in water, glass powder partially crystallised to give valentinite, probably due to the water leaching chlorine from the interface.
- On heating, glasses crystallised to senarmontite and onoratoite, with some valentinite.
- Valentinite in the samples underwent a depressed phase transition to senarmontite, possibly due to initially forming under strain due to the presence of chlorine.
- The other thermal events in the system correspond with those of crystalline onoratoite, including three closely arranged peaks before melting

which may correspond to a three-stage senarmontite-valentinite transition in the sample.

- Kissinger plots suggest that the activation energy required for crystallisation for the 50/50 glasses decreases with sample age, possibly due to the introduction of hydroxyl groups.

5.4 References

[1] G. Thornton, *Acta Crystallogr. B* **33** (1977), 1271-1273.

[2] C. Svensson, *Acta Crystallogr. B* **31** (1975), 2016-2018.

[3] C. Svensson, *Acta Crystallogr. B* **30** (1974), 458-461.

[4] F. Sgarlata, *Period. Mineral.* **39** (1970), 315-328.

[5] G. Mestl, P. Ruiz, B. Delmon and H. Knözinger, *J. Phys. Chem.* **98** (1994), 11276-11282.

[6] C.A. Cody, L. DiCarlo and R.K. Darlington, *Inorg. Chem.* **18**(6) (1979), 1572-1576.

[7] K. Terashima, T. Hashimoto, T. Uchino, S-H. Kim and T. Yoko, *J. Ceram. Soc. Japan* **104**(11) (1996), 1008-1014.

[8] S.A. Jones, J. Fenerty and J. Pearce, *Thermochim. Acta* **114** (1987), 61-66.

[9] S.E. Golunski, T.G. Nevell and M.I. Pope, *Thermochim. Acta* **51** (1981), 153-168.

[10] V.G. Trofimov, A.I. Sheinkman and G.V. Kleshchev, *Izv. Vyssh. Uchebn. Zaved. Fiz.* **3** (1973), 135-137.

[11] F.J. Berry and X. Ren, *J. Mater. Sci.* **39** (2004), 1179-1183.

Chapter 6

Overall Conclusions and Future Work

6.1 Antimony Oxides

6.1.1 The Senarmontite-Valentinite Transition

The senarmontite-valentinite transition in two of the crystalline samples has been observed to occur as a two-stage event, with onset temperatures of 615±3°C and 645±3°C for each stage. In the milled senarmontite, a single transition at 625±3°C was apparent.

There is no evidence to support the value quoted by Roberts and Fenwick [1] of 570±10°C, and doubts expressed earlier about possible sulphur contamination (or other effects from attempted purification) in their sample would appear to be justified. Similarly, Centers' assertion of 556°C for the transition temperature [2] also appears to be in error.

Herein, depression of the phase transition temperature has been attributed to varying amounts of absorbed water in the sample, principally due to small amounts of oxidation observed under inert atmospheres and more extreme depression in the samples quenched by pouring into water (*q.v.* Section 5.2.3). Of the other temperatures reported in the literature (*q.v.* Section 3.1.2) – approximately, 606±5°C [3-5], 629°C [6-7] and 640-655°C [8] – a certain correlation can be seen with the values observed in this work. It can therefore be postulated that previous authors' observations are also based on samples with absorbed water, and it is for this reason that the reported values differ so markedly from each other. The lack of mention of a two-stage transition event may be attributable to the use of less sensitive equipment, and/or to specifics of the mechanism as yet not discovered (it is worth noting, for example, that even at the sampling rate of 10 points per second used in this work, only a single transition peak was observed for the milled senarmontite sample). The onset of melting so soon after the transition is also a complicating factor.

6.1.2 Polymorph Oxidation Temperatures

The mechanically-derived valentinite sample began to oxidise at a temperature of 410±3°C, similar to that reported by Trofimov *et al.* [9]. This is significantly lower than the temperature reported by other authors [7,10] and it seems likely that the discrepancy is due to the smaller particulate size of the valentinite examined herein.

The oxidation temperature observed for the commercial and milled senarmontite samples, 531±4°C, does not appear to correspond to any previously reported value. However, variations due to particulate size between samples is also possible in this case and other factors, such as the amount of oxygen in the local atmosphere and the absorbed water in the sample may also be factors, as may the lowering of oxidation observed by Trofimov *et al.* in mixtures of both Sb_2O_3 polymorphs [9]; it is worth noting that the second stage of oxidation in the water-poured samples, believed to be attributable to senarmontite, occurred at 511±5°C, lower than that displayed for the pure senarmontite samples.

6.1.3 Melting Point of Sb_2O_3

The melting point observed in the three crystalline samples, 652±5°C, is entirely consistent with the temperature most commonly given for antimony trioxide. However, the melting temperature of 640±6°C measured for the water-poured samples suggests that the values quoted by Golunski *et al.* [7] may still bear merit – again, the effects of absorbed water may be significant. There is, however, no evidence to support Jones *et al.* [8] in their report of a variation in the melting temperature with heating rate.

6.1.4 Mechanically-derived Valentinite

The preparation of valentinite by mechanical milling reported by Berry and Ren [11] appears to be a valid method of producing pure samples of this polymorph, with one caveat: the resultant material appears, based on XRD data and the depression of the phase transition to senarmontite, to be formed under strain, which may affect its usefulness. However, the process has advantages in avoiding the potential for oxidation and volatilisation during standard thermal preparations.

6.1.5 Sb_2O_4

As mentioned briefly in Section 5.1.1, three peaks were observed in the diffraction pattern of cervantite that do not correspond to single-crystal reference studies. Subsequent to the investigations detailed in this work, and following the observation of unusual time-dependent behaviour in NMR results, Holland [5] conducted further XRD analysis of the substance over time. That study has identified five additional peaks not corresponding to the cervantite reference pattern, and has identified an age-dependent correlation with their relative intensities (Fig. 6.01). The peaks appear to correspond to a hydrate of Sb_2O_5 and to clinocervantite (the alternate polymorph of Sb_2O_4).

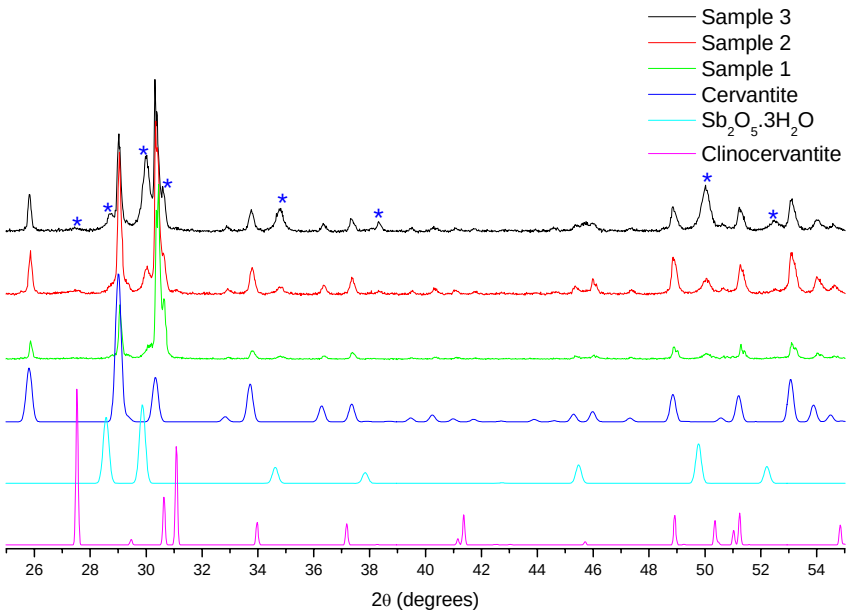

Figure 6.01 *– The XRD patterns obtained by Holland [5] in a study of commercial Sb_2O_4 (cervantite) over time (samples 1-3 are numbered in order of age). Reference patterns for cervantite (blue) [12], $Sb_2O_5.3H_2O$ (cyan) [13] and clinocervantite (magenta) [14] are also shown. Starred peaks are those that do not correspond with the cervantite pattern, and increase with sample age.*

6.2 Water-quenched Antimony Oxide Glass

Quenching molten Sb_2O_3 by pouring the melt into water appears to be a valid method of producing glass. Although only 52% of each sample examined in this work appeared to be vitreous, it is to be expected that refinement of the quenching process (by e.g. regulating the rate of pouring, lowering the temperature of the water, reducing the sample size, etc.) would produce more uniformly glassy products. As to be

expected from the rapid cooling process, the majority of the crystalline formation of the samples was the high-temperature stable valentinite.

There was evidence that the valentinite present in the samples was under strain, and thus underwent a depressed phase transition to senarmontite. This would be consistent with the crystallisation of the glass, where senarmontite is the majority crystalline product, suggesting that the formation of valentinite is not favoured by the high water content and thus that which is produced as a result is less stable than normal; the valentinite formed on initial quenching of the melt would behave similarly.

As with the crystalline samples, the senarmontite-valentinite phase transition was observed to be depressed in the material crystallised from the glasses. However, the temperature shift is of higher magnitude and the transition appears to take place in a single stage, further suggesting a correlation with the amount of water present in the crystalline material. The presence of water is known to increase the kinetics of phase transformations by introducing M-OH groups which break M-O-M linkages, and this may be the case here as well.

Oxidation and melting of the samples has been commented upon earlier (Sections 6.1.2 and 6.1.3, respectively); it is most significant to note that there are discrepancies with the crystalline oxides here also. Overall, the stability of the glass produced by this method is low (as to be expected from the extreme cooling method required) with $T_C - T_g = 55\text{-}60°\text{C}$.

6.3 Chlorine-stabilised Antimony Oxide Glasses

Formation of glass from mixtures of Sb_2O_3 and $SbCl_3$ by splat-quenching appear to be entirely feasible, confirming the work of Johnson *et al.* [15-16]. Preparations of $xSb_2O_3(1\text{-}x)SbCl_3$ with x = 0.5, 0.7 and 0.85 all met with success, although it is interesting to note that the mixtures with the highest initial chlorine content (x = 0.5) were the only melts to fully vitrify on cooling, yet produced glasses with the lowest levels of chlorine of those studied (the x = 0.85 melts phase-separated on cooling, with the minority forming a purely glassy phase, but with a higher chlorine content). The x = 0.5 glasses also appeared to be slightly more stable, albeit still less so than the water-poured glasses, with $T_C - T_g = 45\text{-}52°\text{C}$: some 10°C higher than for the other chlorine-stabilised preparations. Valentinite and onoratoite were the principal crystalline

products of those melts that did not fully vitrify, although there was also some evidence of senarmontite formation on the surface (only) of some of the glasses.

The glasses demonstrate some sensitivity to moisture (although far less extreme than that of $SbCl_3$) with immersion in water forming a layer of valentinite on the surface of the material. Raman spectroscopy data suggests that the glasses have a structure most similar to that of onoratoite, and the valentinite formation appears consistent with chlorine being leached from the surface layer. Further indications of moisture-sensitivity are given by the apparent decrease in crystallisation activation energy with age in the 50/50 glasses, which may suggest the introduction of hydroxyl groups.

Crystallisation of the glasses through heating produced senarmontite and onoratoite, with some valentinite, and was followed at higher temperature by the latter experiencing a depressed transition to senarmontite, as with the water-poured samples (*q.v.* Section 6.2). This feature may be consistent with the formation of strained valentinite due to the presence of chlorine, analogous to the water-induced strain proposed for the water-poured glasses, or with the effect of M-Cl bonds on the kinetics (in a similar fashion to the influence of M-OH bonds when water is introduced).

After the endothermic event related to the thermal decomposition of onoratoite, three consecutive and partially overlapping events were detected prior to melting of the samples. Based on the observations of the previous systems in this work, it is suggested that these correspond to a multi-stage senarmontite-valentinite transition, due to the formation of strained senarmontite at various stages in the thermal history of the sample.

6.4 Future Work

Several avenues of further investigation present themselves as result of this study:

- The presence of absorbed water appears to depress the temperature of the phase transition in the senarmontite system – there are also changes to the oxidation and melting temperatures in the Sb_2O_3 crystallised from water-poured glasses. A study to confirm the influence of water in these systems, and to determine the relevant mechanism and dependence (if any) on the amount of water present could be conducted through the use of XRD, ^{1}H and ^{17}O NMR

and STA techniques. The effect (especially on oxidation) of particulate size could be examined as an additional variable, and ^{1}H and ^{17}O NMR together with neutron diffraction techniques could also be employed to obtain structural information on the water-poured glasses (with D_2O in place of water for the neutron diffraction measurements).

- The activation energy of crystallisation appears to decrease with age in the chlorine-stabilised glasses, possibly as a result of interaction with atmospheric moisture. Further kinetic studies of this and other thermal events in the systems studied in this work, using DSC techniques and accounting for the volatilisation of the samples above ~500°C, could be useful.
- There appears to be a time-dependent change in the structure of the commercial cervantite used in this study. A further investigation into this change, using XRD, NMR and Mössbauer spectroscopy, could be undertaken on this substance – which is usually regarded as the most stable of the antimony oxides.
- Although the general identity of the three pre-melting events in the chlorine-stabilised antimony oxide glass system have been inferred in this work, high-temperature XRD, Raman spectroscopy and neutron diffraction could be used to properly identify the nature of these events, potentially giving insights into the effects of chlorine in this system. These techniques could also be used to attempt to extract more information from the glass crystallisation event, and may also give structural insights into the glass system.
- Finally, although not possible in this work due to time constraints, EDX measurements on onoratoite to use as a reference for the chlorine content measured in the chlorine-stabilised glass samples would also be logical.

6.5 References

[1] E.J. Roberts and F. Fenwick, *J. Amer. Chem. Soc.* **50** (1928), 2125-2147.

[2] P.W. Centers, *J. Solid State Chem.* **72** (1988), 303-308.

[3] Y.K. Agrawal, A.L. Shashimohan and A.B. Biswas, *J. Therm. Anal.* **7** (1975), 635-641.

[4] W.B. White, F. Dachille and R. Roy, *Z. Krist.* **125** (1967), 450-458.

[5] D. Holland (personal communication).

[6] S.E. Golunski and D. Jackson, *Appl. Catal.* **48** (1989), 123-135.

[7] S.E. Golunski, T.G. Nevell and M.I. Pope, *Thermochim. Acta* **51** (1981), 153-168.

[8] S.A. Jones, J. Fenerty and J. Pearce, *Thermochim. Acta* **114** (1987), 61-66.

[9] V.G. Trofimov, A.I. Sheinkman and G.V. Kleshchev, *Izv. Vyssh. Uchebn. Zaved. Fiz.* **3** (1973), 135-137.

[10] C.A. Cody, L. DiCarlo and R.K. Darlington, *Inorg. Chem.* **18**(6) (1979), 1572-1576.

[11] F.J. Berry and X. Ren, *J. Mater. Sci.* **39** (2004), 1179-1183.

[12] G. Thornton, *Acta Crystallogr. B* **33** (1977), 1271-1273.

[13] W.A. England, M.G. Cross, A. Hamnett, P.J. Wiseman and J.B. Goodenough, *Solid State Ionics* **1** (1980), 231-249.

[14] R. Basso, G. Lucchetti, L. Zefiro and L. Palenzona, *Eur. J. Mineral.* **11** (1999), 95-100.

[15] J.A. Johnson, D. Holland, J. Urquidi, I.A. Gee, C.J. Benmore and C.E. Johnson, *J. Phys.: Condens. Matter* **15** (2003), 4679-4693.

[16] J.A. Johnson, D. Holland, J. Bland, C.E. Johnson and M.F. Thomas, *J. Phys.: Condens. Matter* **15** (2003), 755-764.